Electronic Supplementary Material (ESI) for Green Chemistry.

Supplementary Material

Insights into the reaction network and kinetics of xylose conversion over combined Lewis/Brønsted acid catalysts in a flow microreactor

Wenze Guo, [a, b] Herman Carolus Bruining, [a] Hero Jan Heeres,[a] Jun Yue[a,*]

[a] *Department of Chemical Engineering, Engineering and Technology Institute Groningen, University of Groningen, Nijenborgh 4, 9747 AG Groningen, The Netherlands*

[b] *State Key Laboratory of Chemical Engineering, Department of Chemical Engineering, East China University of Science and Technology, Shanghai 200237, PR China*

* Corresponding author:

Jun Yue (yue.jun@rug.nl)

Table of contents

S1. Experimental conditions for kinetic experiments in monophasic water in microreactors

Table S1. Experimental conditions for kinetic experiments in monophasic water in microreactors

T (°C)	Catalyst	Starting substrate
120	200 mM HCl	0.1 M xylose, 0.1 M lyxose, 0.01 M xylulose, 0.1 M furfural
	40 mM $AlCl_3$	0.1 M xylose, 0.1 M lyxose, 0.01 M xylul ose, 0.1 M furfural
140	200 mM HCl	0.1 M xylose, 0.1 M lyxose, 0.01 M xylulose, 0.1 M furfural
	40 mM $AlCl_3$	0.1 M xylose, 0.1 M lyxose, 0.01 M xylulose, 0.1 M furfural
160	40 mM $AlCl_3$	0.1 M xylose, 0.3 M xylose, 0.5 M xylose, 0.1 M lyxose, 0.3 M lyxose, 0.5 M lyxose, 0.01 M xylulose, 0.03 M xylulose, 0.05 M xylulose, 0.1 M furfural, 0.3 M furfural, 0.5 M furfural
	80 mM $AlCl_3$	0.1 M xylose, 0.1 M lyxose, 0.01 M xylulose, 0.1 M furfural
	120 mM $AlCl_3$	0.1 M xylose, 0.1 M lyxose, 0.01 M xylulose, 0.1 M furfural
	19 mM HCl	0.1 M xylose, 0.1 M lyxose, 0.01 M xylulose, 0.1 M furfural
	50 mM HCl	0.1 M xylose, 0.1 M lyxose, 0.01 M xylulose, 0.1 M furfural
	100 mM HCl	0.1 M xylose
	40 mM $AlCl_3$ + 100 mM HCl	0.1 M xylose
	80 mM $AlCl_3$ + 100 mM HCl	0.1 M xylose
	120 mM $AlCl_3$ + 100 mM HCl	0.1 M xylose
	200 mM $AlCl_3$ + 100 mM HCl	0.1 M xylose
	200 mM HCl	0.1 M xylose, 0.3 M xylose, 0.5 M xylose, 0.1 M lyxose, 0.3 M lyxose, 0.5M lyxose 0.01 M xylulose, 0.03 M xylulose, 0.05 M xylulose, 0.1 M furfural, 0.3 M furfural, 0.5 M furfural
	400 mM HCl	0.1 M xylose, 0.1 M lyxose, 0.01 M xylulose, 0.1 M furfural
180	200 mM HCl	0.1 M xylose, 0.1 M lyxose, 0.01 M xylulose, 0.1 M furfural
	40 mM $AlCl_3$	0.1 M xylose, 0.1 M lyxose, 0.01 M xylulose, 0.1 M furfural

S2. Quantification of xylulose and lyxose using a Gaussian deconvolution method

The retention times for xylulose and lyxose on HPLC chromatogram are 12.9 min and 13.0 min, respectively (Figure S1a). Such a similar retention time for these species leads to a severe overlap of their peaks (Figure S1b). To determine the area of the peaks of xylulose and lyxose, a Gaussian deconvolution method was applied by fixing the position of the fitted peaks of xylulose and lyxose, with the intensity of these peaks adjusted to keep the position and FWHM (full width at half maximum) of the overall fitted curve nearly identical to the experimental curve (Figure S1b). The above curving fitting process was performed on an OriginPro 8.5 Software (OriginLab Corporation). Then, the concentrations of xylulose and lyxose were calculated using the calibration equations obtained from the standard solutions of known compound with known concentrations.

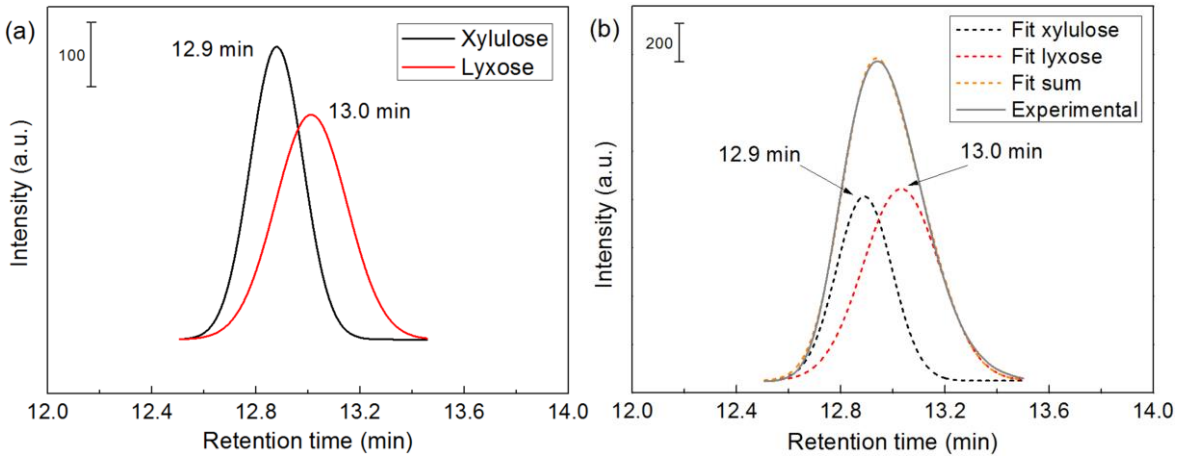

Fig. S1. (a) HPLC chromatogram of the individual standard xylulose and lyxose; (b) analysis of the compounds using deconvolution method on the HPLC chromatogram of the product sample. Reaction conditions: 0.1 M xylose, 40 mM $AlCl_3$, 160 °C and 2 min.

S3. The volumetric flow rate change and ratio of the aqueous or organic phase after mixing and reaction

S3.1 Flow rate change and ratio between the microreactor inlet and outlet at 20 °C

Under the conditions that the aqueous phase and MIBK phase were mixed and then separated at 20 ˚C, the simulation results of the flow rate changes were summarized in Table S2. In the table, γ_{aq} or γ_{org} represents the ratio of the volumetric flow rates of the aqueous or organic phase between the microreactor outlet and inlet (both at ca. 20 °C). The value of this ratio was estimated using Aspen Plus simulation, the details of which has been reported in our previous work.[1]

Table S2. Volumetric flow rate change and ratio of the aqueous or organic phase after mixing, reaction and cooling to 20 °C according to the Aspen Plus simulation.

Inlet volumetric flow rate ratio (MIBK : water)	Q_{org} (mL/min)		γ_{org} (-)	Q_{aq} (mL/min)		γ_{aq} (-)
	Inlet[a] (20 °C)	Outlet[b] (20 °C)		Inlet[a] (20 °C)	Outlet[b] (20 °C)	
4:1	400	400.78	1.002	100	96.46	0.965
2:1	200	199.13	0.996	100	99.48	0.995
1:1	100	98.30	0.983	100	100.99	1.010
1:2	100	95.77	0.958	200	203.49	1.018
1:4	100	90.70	0.907	400	408.48	1.021

[a] Before mixing, each phase was fed at 20 °C.

[b] After two-phase mixing and separation at 20 °C.

S3.2 Flow rate change and ratio of each phase between 20 °C and the reaction temperature (*T*)

Due to the temperature-dependency of the liquid density and partial miscibility between water and MIBK, the volumetric flow rate of the aqueous or organic phase changed after two-phase mixing and heating-up from 20 °C to reaction temperature (*T*). Such a flow rate change

was estimated by Aspen Plus Simulation as reported in our previous work.[1-3] The flow rate change ratio ($\alpha_{\mathrm{bi,aq}}$ or $\alpha_{\mathrm{bi,org}}$) was approximated as eqn 17 ($Q_{\mathrm{aq}} = Q_{\mathrm{aq,\,0}}\alpha_{\mathrm{mono,\,aq}}$), where the parameters are given in Table S3.

Table S3. Values of the model parameters in eqn 17.[2]

Ratio	Initial O/A[a]	*u*	*v*	*w*
(-)	(-)	(-)	(-)	(-)
$\alpha_{\mathrm{bi,aq}}$	1	0.870	0.129	0.004
	2	0.898	0.092	0.003
	3	0.983	-0.001	0.014
	4	1.013	-0.040	0.006
$\alpha_{\mathrm{bi,org}}$	1	0.755	0.205	0.006
	2	0.781	0.193	0.006
	3	0.789	0.188	0.006
	4	0.793	0.187	0.006

[a] Before mixing, each phase was fed at 20 °C.

S4. Quantification of aluminum species and H^+ in water

$AlCl_3$ readily hydrolyzes stepwise in water to form various species such as $[Al(H_2O)_6]^{3+}$, $[Al(OH)(H_2O)_5]^{2+}$, $[Al(OH)_2(H_2O)_4]^{+}$, $Al(OH)_3$, and $[Al(OH)_4]^{-}$, as expressed in eqn S1-S6. These aluminum species are in equilibrium with each other, of which the amount depends on the temperature (*T*), pH value (or equivalently, the HCl concentration C_{HCl}), and $AlCl_3$ concentration ($C_{\mathrm{AlCl_3}}$).

$$\mathrm{Al^{3+} + H_2O \xleftrightarrow{K_1} Al(OH)^{2+} + H^+} \quad \text{(S1)}$$

$$\mathrm{Al^{3+} + 2H_2O \xleftrightarrow{K_2} Al(OH)_2^{+} + 2H^+} \quad \text{(S2)}$$

$$\mathrm{Al^{3+} + 3H_2O \xleftrightarrow{K_3} Al(OH)_3^{0} + 3H^+} \quad \text{(S3)}$$

$$Al^{3+} + 4H_2O \xleftrightarrow{K_4} Al(OH)_4^- + 4H^+ \quad \text{(S4)}$$

For each hydrolysis reaction mentioned above, the equilibrium constants (K_i) are defined as

$$K_i = \frac{[Al(OH)_i^{(3-i)+}][H^+]^i}{[Al]^{3+}} \quad \text{(S5)}$$

where i = 1, 2, 3 and 4, corresponding to eqn S1-S4, respectively. The values of K_i are calculated via an empirical equation[4]

$$\log_{10} K_i = a + b\log_{10} T + c/T \quad \text{(S6)}$$

Here, T (in K) is the temperature, and the polynomial coefficients a, b and c for K_i are listed in Table S4.

Table S4. Polynomial coefficients for the estimation of K_i values from 0-300 °C[4]

K_i	a	b	c
K_1	153.578	52.9073	5271.05
K_2	78.6758	28.9013	-883.083
K_3	41.943	-10.1134	-9851.53
K_4	22.3129	9.72248	-7125.85

In aqueous system with known concentrations of $AlCl_3$ (C_{AlCl_3}) and HCl (C_{HCl}), there is according to mole balances for both aluminum species and H^+

$$C_{AlCl_3} = C_{Al^{3+}} + C_{Al(OH)^{2+}} + C_{Al(OH)_2^+} + C_{Al(OH)_3^0} + C_{Al(OH)_4^-} \quad \text{(S7)}$$

$$C_{H^+} = C_{HCl} + C_{Al(OH)^{2+}} + 2C_{Al(OH)_2^+} + 3C_{Al(OH)_3^0} + 4C_{Al(OH)_4^-} \quad \text{(S8)}$$

Therefore, for the given known reaction temperature (T) and concentrations of $AlCl_3$ and HCl, the concentrations of each aluminum species and H^+ can be determined by combining eqn S5-S8. For example, the concentrations of $Al(OH)_2^+$ and H^+ under some representative conditions are listed in Table S5 hereafter (Section S8).

S5. Comparison of the conversion of xylose, xylulose and lyxose using HCl as the catalyst

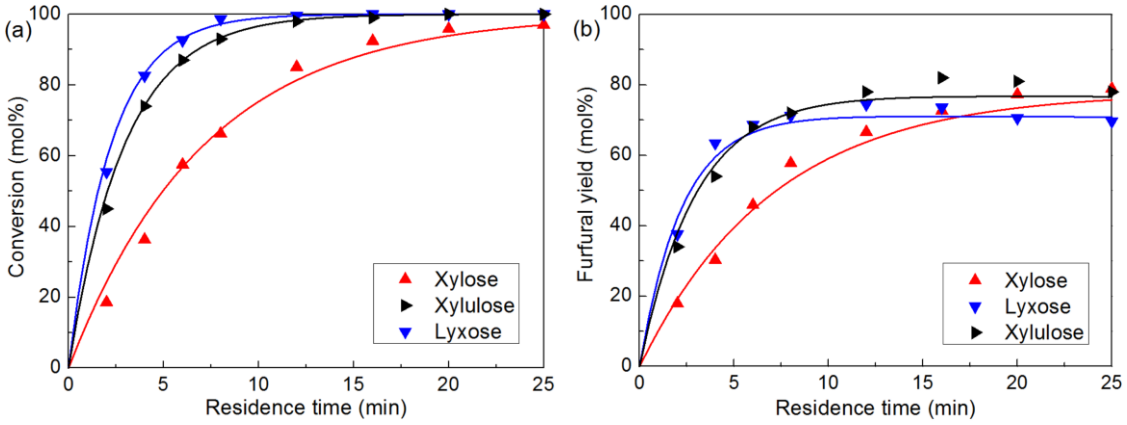

Fig. S2. (a) Sugar conversion and (b) furfural yield with different hexoses (xylose, xylulose and lyxose) as the substrate over HCl in a water-MIBK biphasic solvent system in the microreactor. Reaction conditions: *L* = 3.3 m, 160 °C, 200 mM HCl, 0.1 M substrate, O/A = 4.

S6. ESI-MS spectra of the aqueous solution of xylose

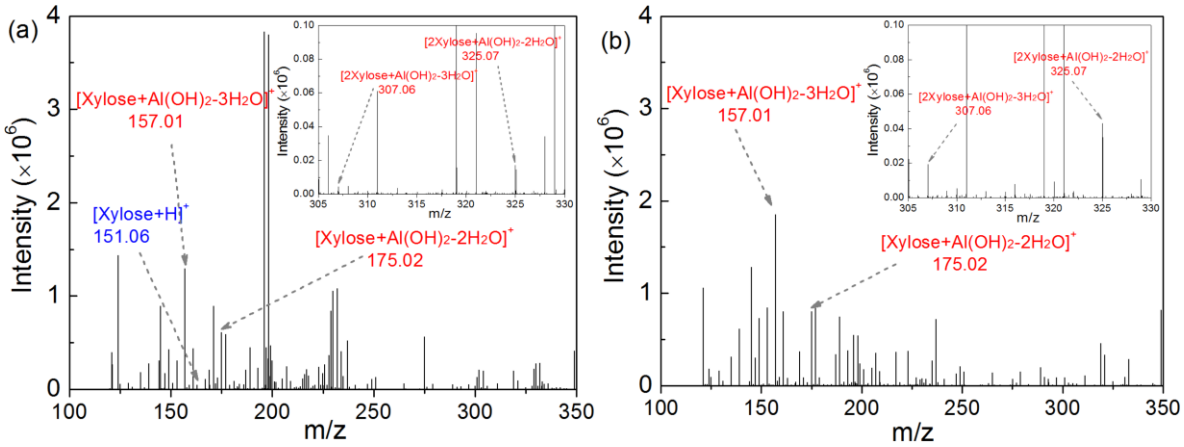

Fig. S3. ESI-MS spectra of the aqueous solution of xylose containing (a)200 mM HCl and 40 mM $AlCl_3$; and (b) 200 mM HCl and 80 mM $AlCl_3$. Inset in (b) shows a magnified view of m/z region at 305-330.

S7. Screening of reaction conditions for the conversion of xylose, lyxose, xylulose and furfural in monophasic water in the microreactor

S7.1 Effect of temperature

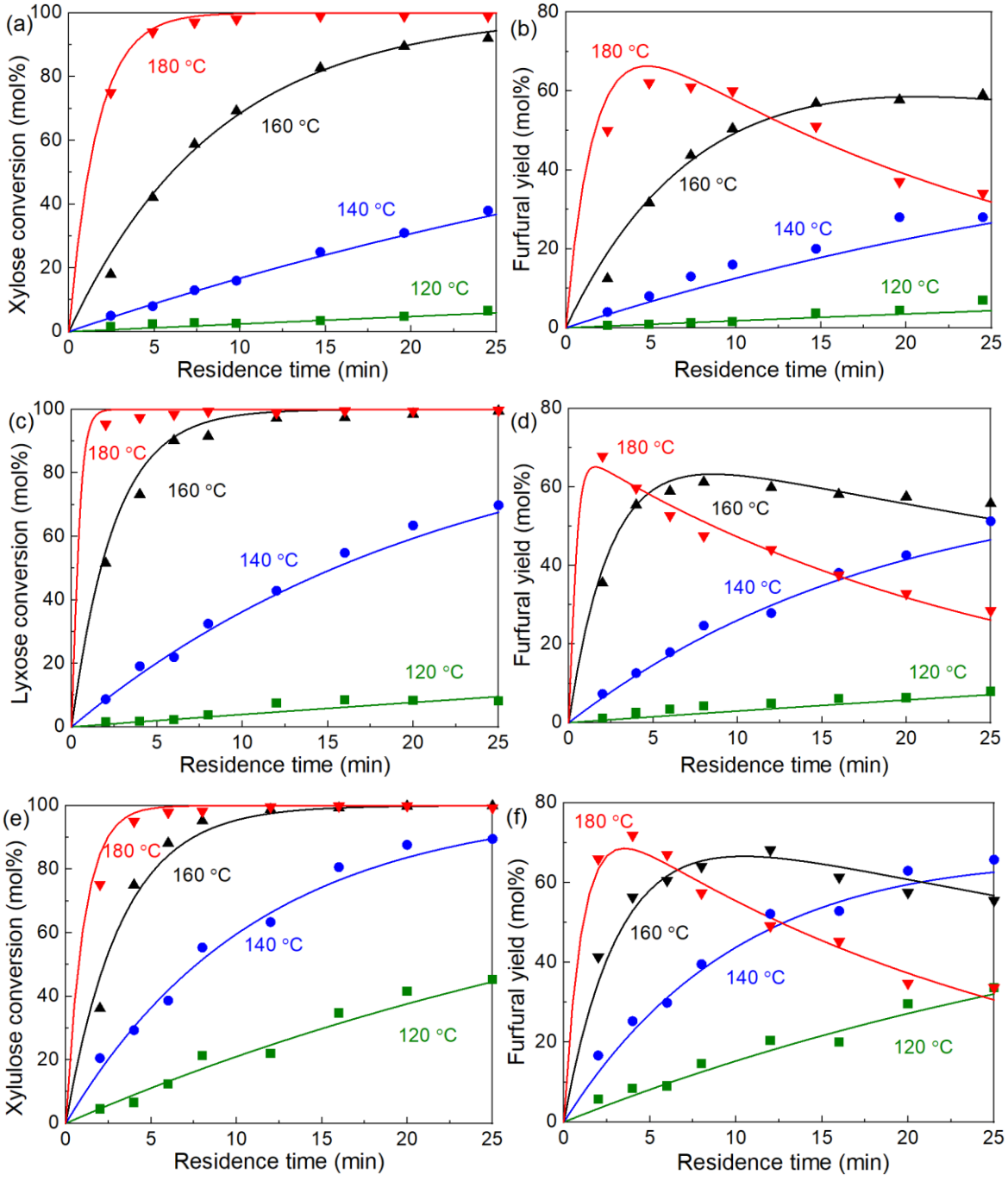

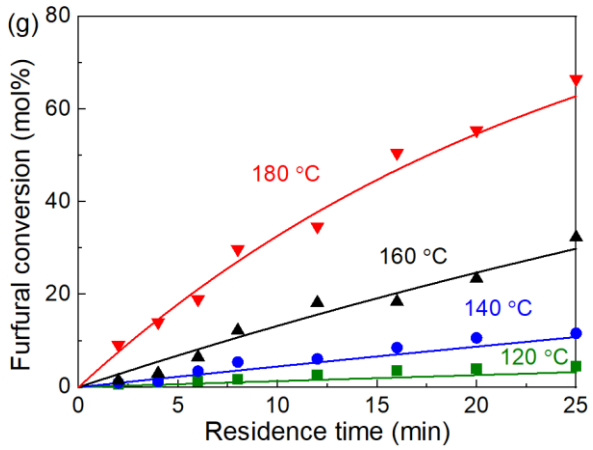

Fig. S4. Effect of temperature on the HCl-catalyzed conversion of sugars or furfural in water in the microreactor. (a) Sugar conversion and (b) furfural yield with xylose as the substrate; (c) sugar conversion and (d) furfural yield with lyxose as the substrate; (e) sugar conversion and (f) furfural yield with xylulose as the substrate; and (g) conversion of furfural as the substrate. Reaction conditions: *L* = 3.3 m, 0.2 M HCl, substrate concentration at 0.01 M for xylulose and 0.1 M for the rest.

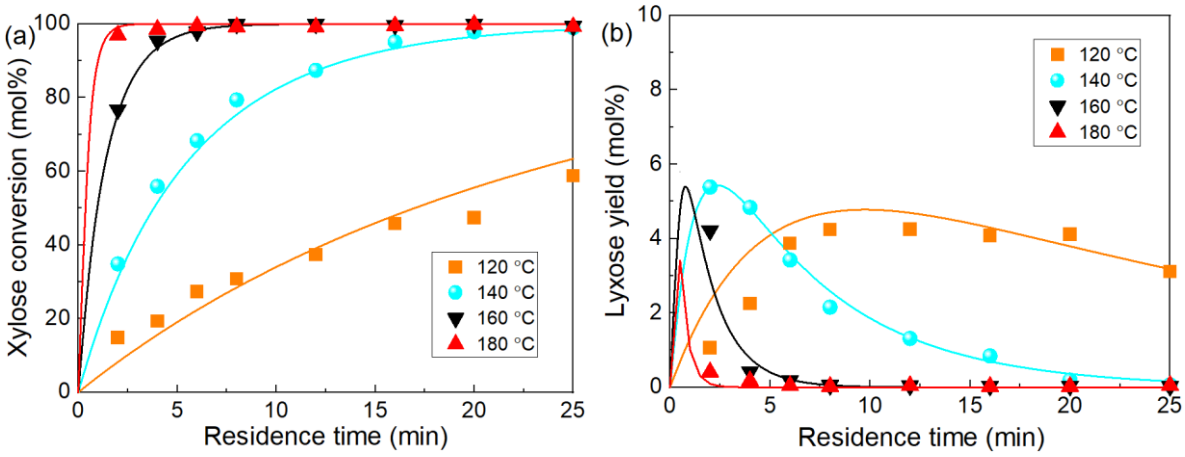

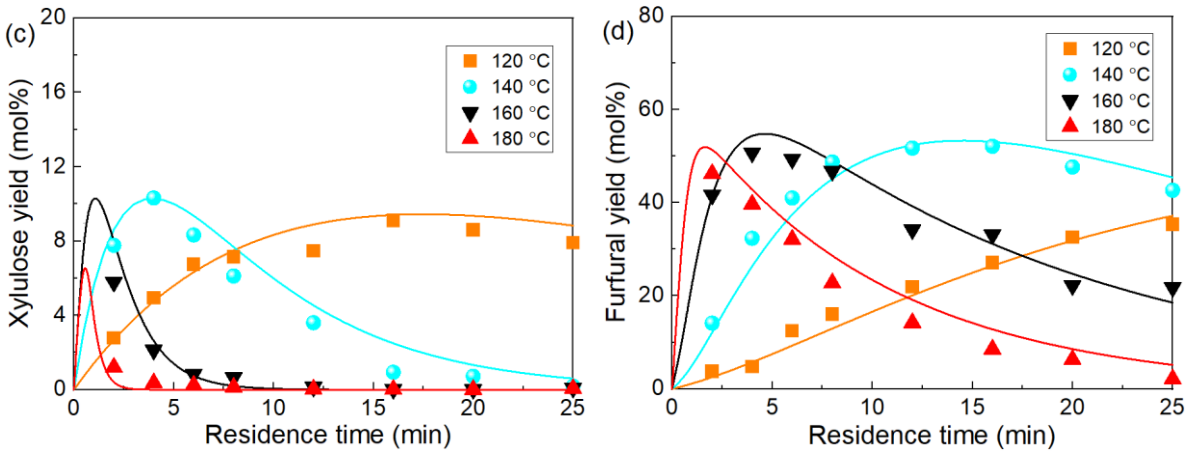

Fig. S5. Effect of temperature on the $AlCl_3$-catalyzed xylose conversion in water in the microreactor. (a) Xylose conversion; (b) lyxose yield; (c) xylulose yield and (d) furfural yield. Reaction conditions: *L* = 3.3 m, 40 mM $AlCl_3$, 0.1 M xylose.

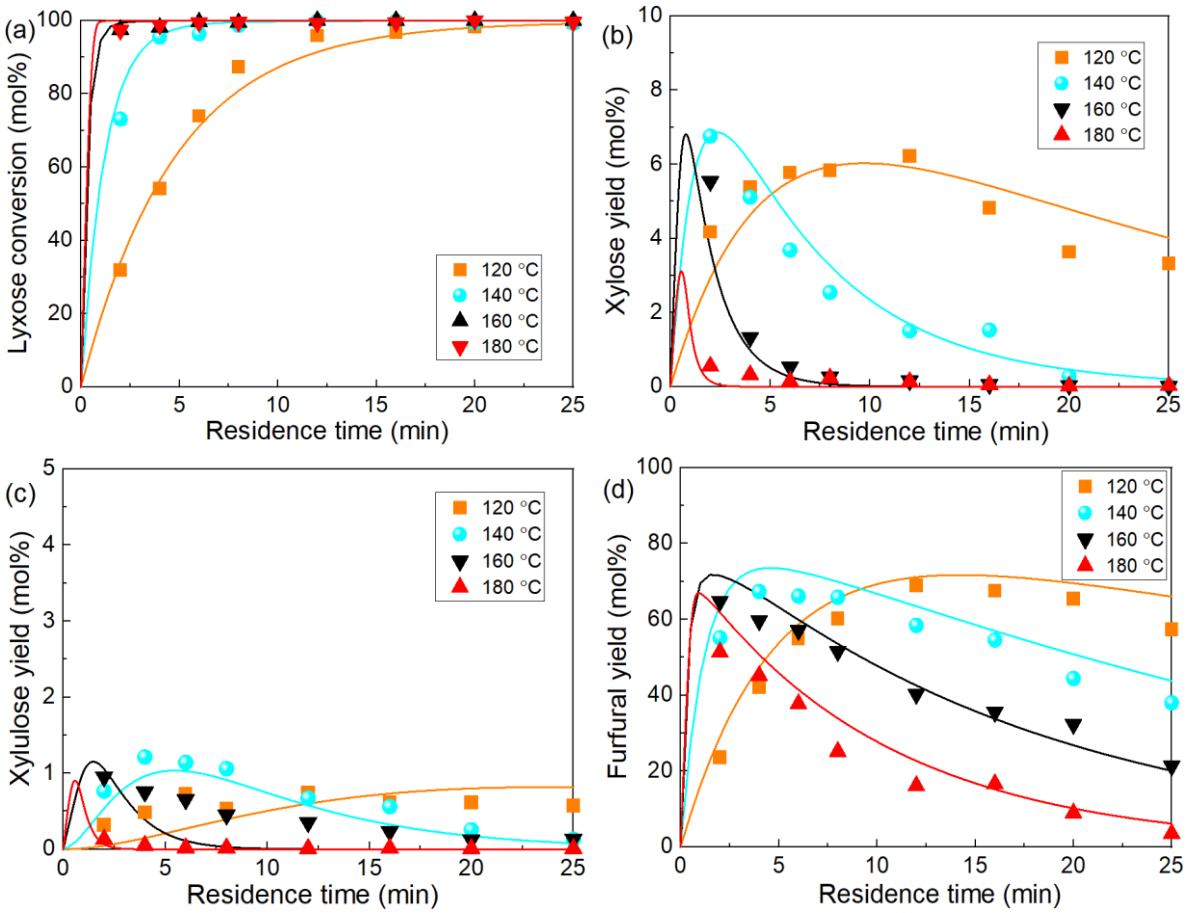

Fig. S6. Effect of temperature on the $AlCl_3$-catalyzed lyxose conversion in water in the microreactor. (a) Lyxose conversion; (b) xylose yield; (c) xylulose yield and (d) furfural yield. Reaction conditions: *L* = 3.3 m, 40 mM $AlCl_3$, 0.1 M lyxose.

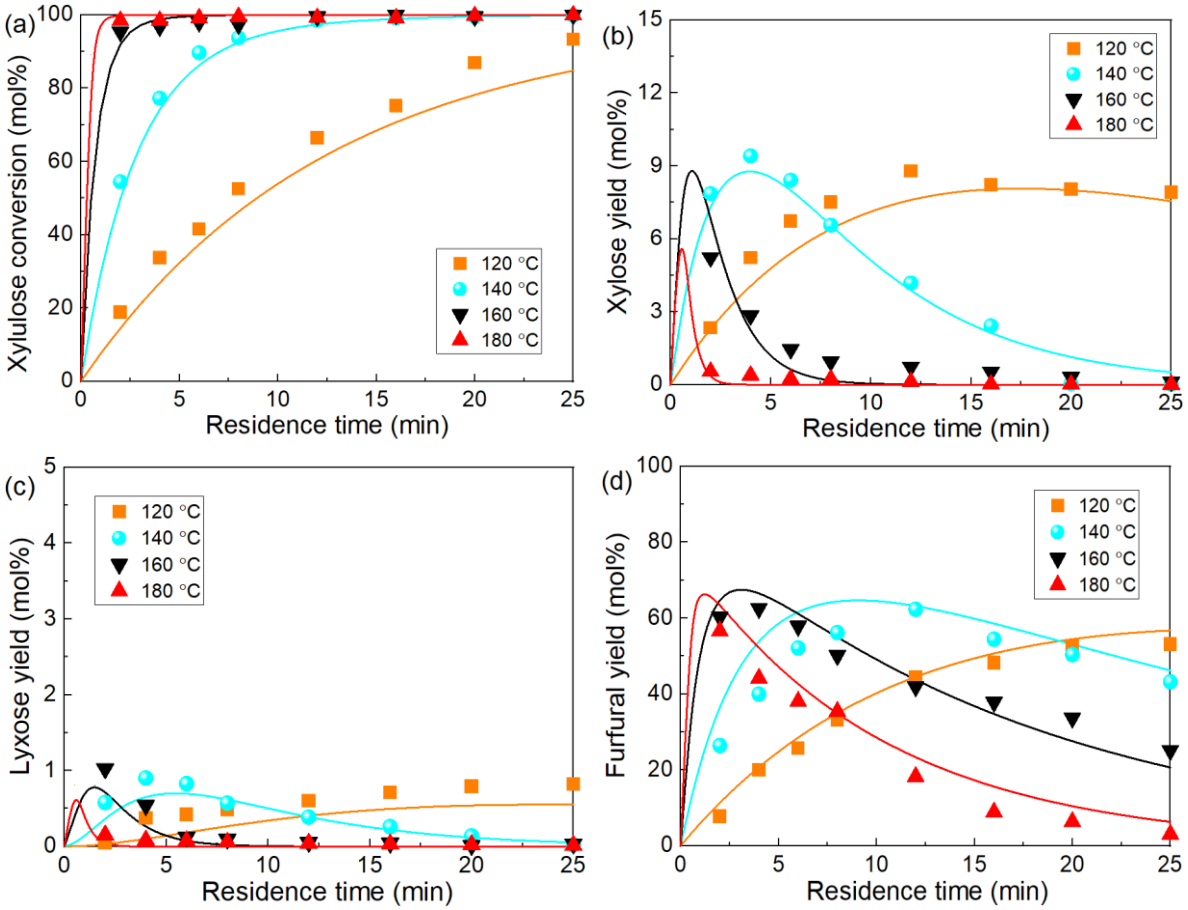

Fig. S7. Effect of temperature on the $AlCl_3$-catalyzed xylulose conversion in water in the microreactor. (a) xylulose conversion; (b) xylose yield; (c) lyxose yield and (d) furfural yield. Reaction conditions: *L* = 3.3 m, 40 mM $AlCl_3$, 0.01 M xylulose.

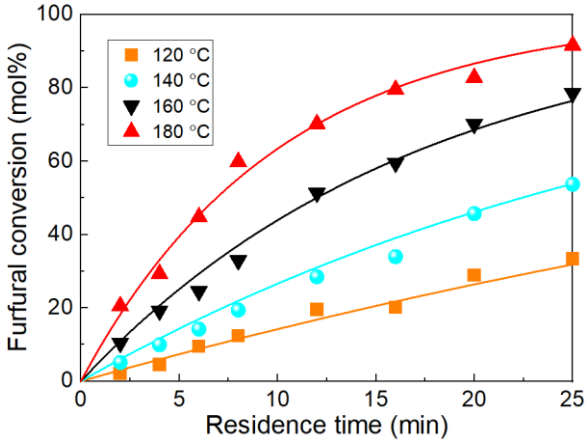

Fig. S8. Effect of temperature on the $AlCl_3$-catalyzed furfural conversion in water in the microreactor. Reaction conditions: *L* = 3.3 m, 40 mM $AlCl_3$, 0.1 M furfural.

S7.2 Effect of acid concentration

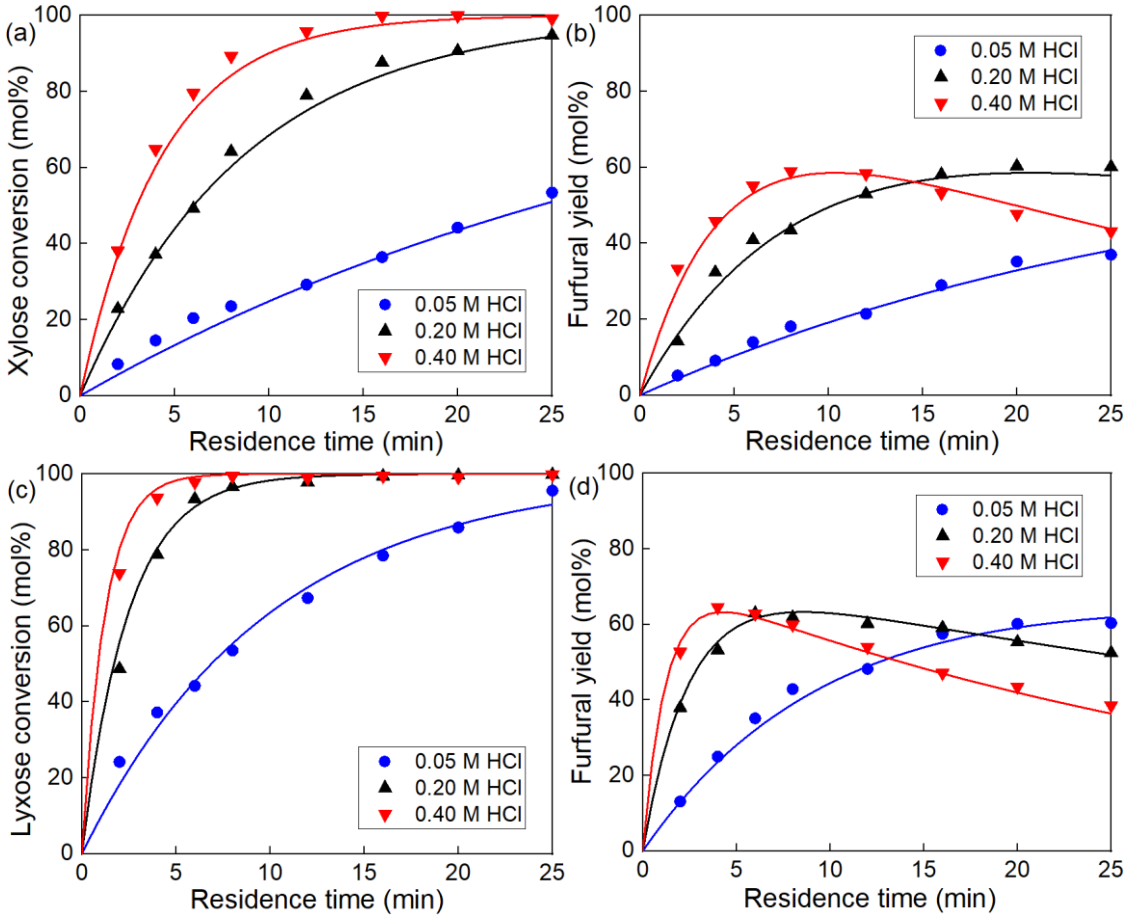

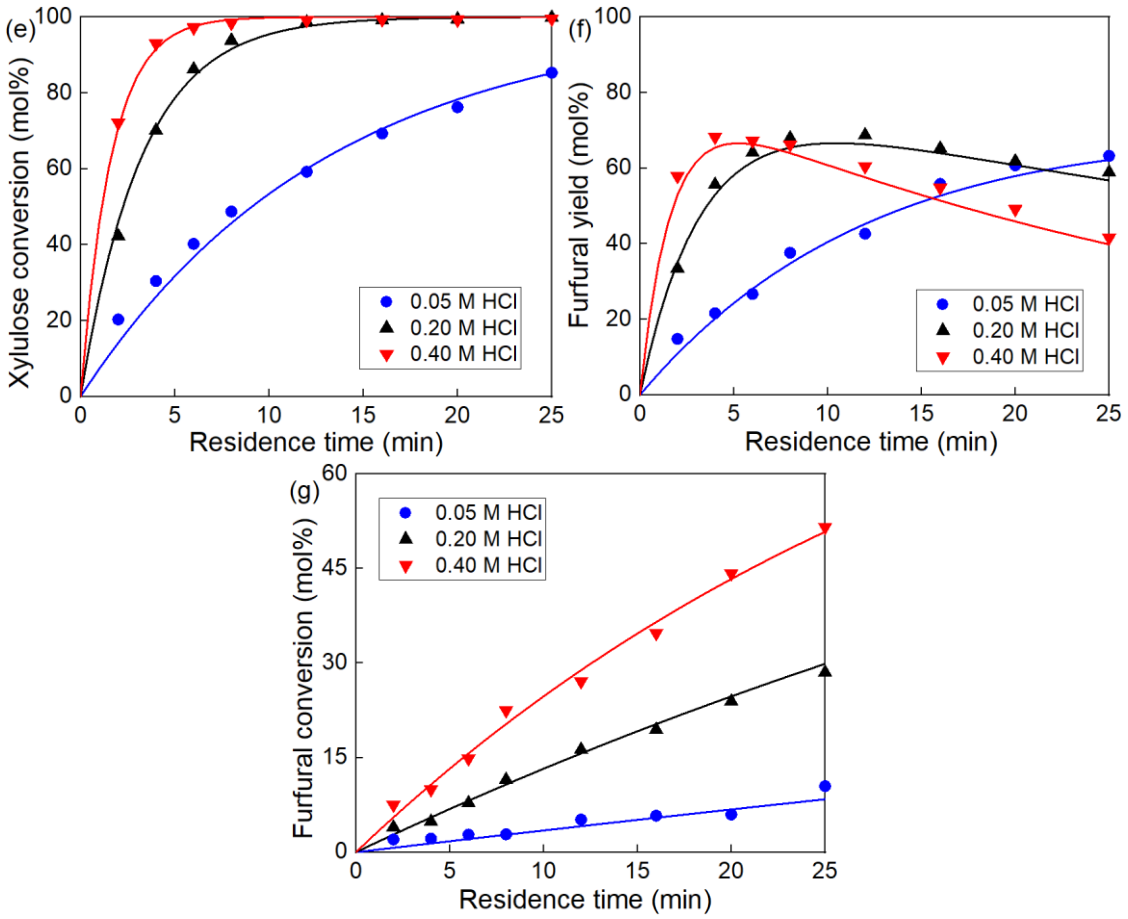

Fig. S9. Effect of acid concentration on the HCl-catalyzed conversion of sugars and furfural. . (a) Sugar conversion and (b) furfural yield with xylose as the substrate; (c) sugar conversion and (d) furfural yield with lyxose as the substrate; (e) sugar conversion and (f) furfural yield with xylulose as the substrate; and (g) conversion of furfural as the substrate. Reaction conditions: *L* = 3.3 m, 160 °C, substrate concentration at0.01 M for xylulose and 0.1 M for the rest.

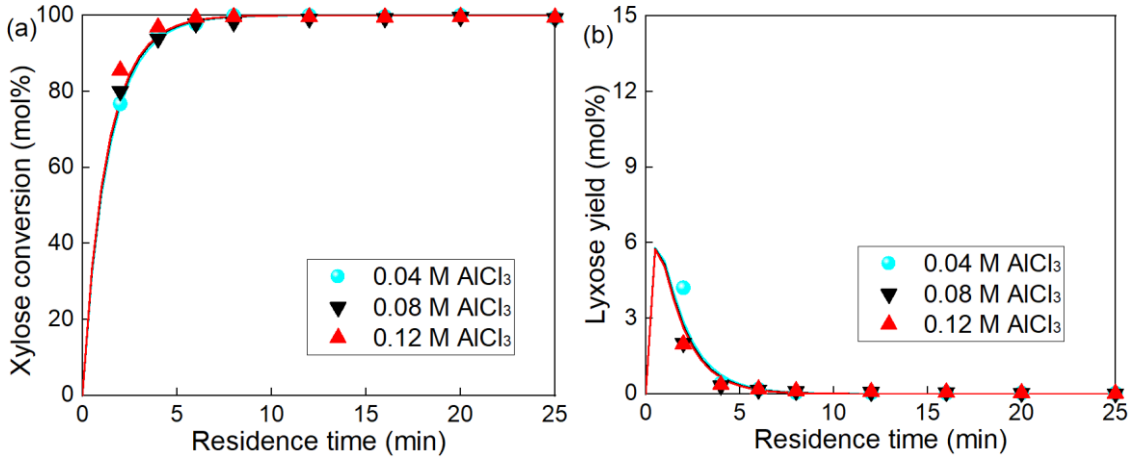

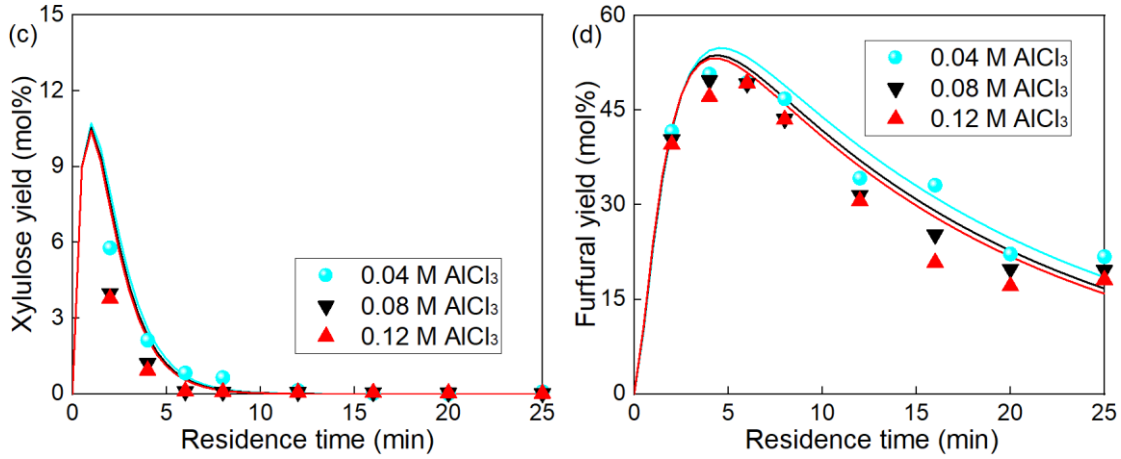

Fig. S10. Effect of acid concentration on the $AlCl_3$-catalyzed xylose conversion. (a) Xylose conversion; (b) lyxose yield; (c) xylulose yield and (d) furfural yield. Reaction conditions: *L* = 3.3 m, 160 °C, 0.1 M xylose.

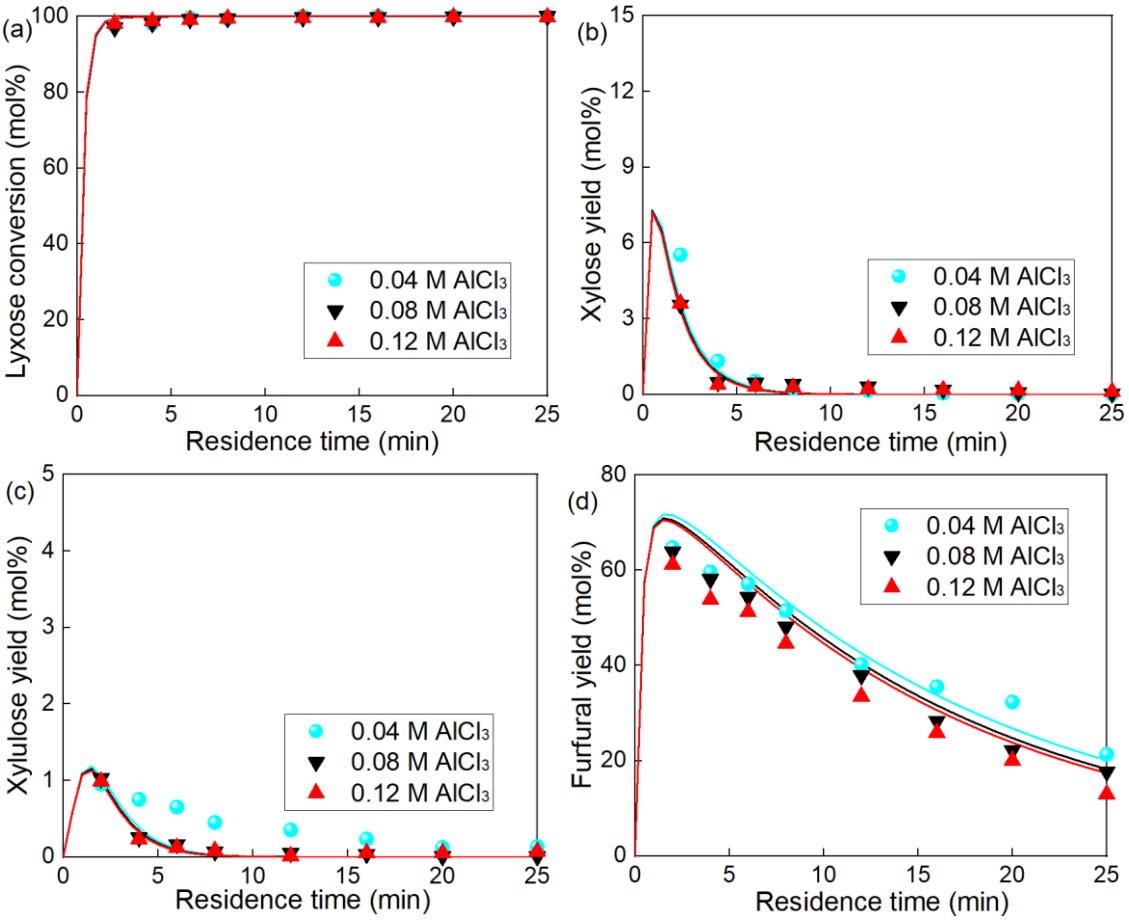

Fig. S11. Effect of acid concentration on the $AlCl_3$-catalyzed lyxose conversion. (a) lyxose conversion; (b) xylose yield; (c) xylulose yield and (d) furfural yield. Reaction conditions: *L* = 3.3 m, 160 °C, 0.1 M lyxose.

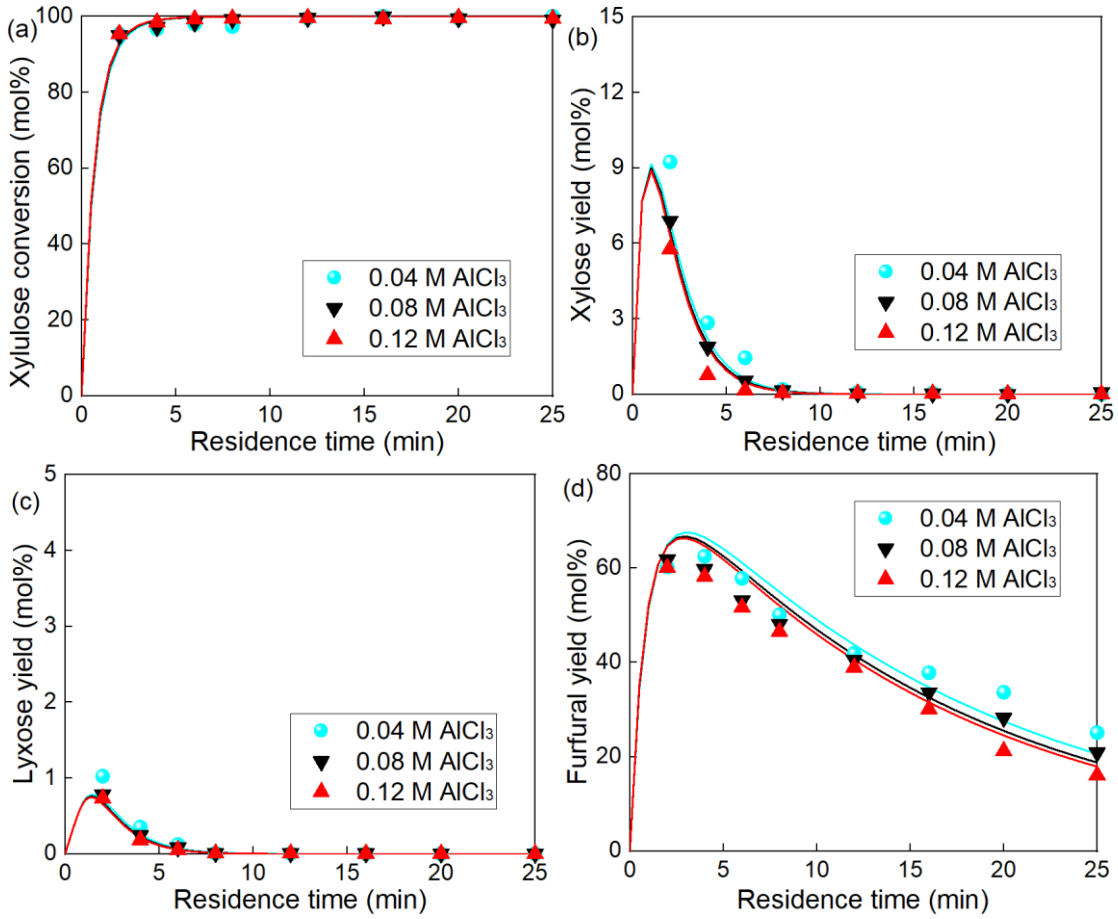

Fig. S12. Effect of acid concentration on the $AlCl_3$-catalyzed xylulose conversion. (a) xylulose conversion; (b) xylose yield; (c) lyxose yield and (d) furfural yield. Reaction conditions: *L* = 3.3 m, 160 °C, 0.01 M lyxose.

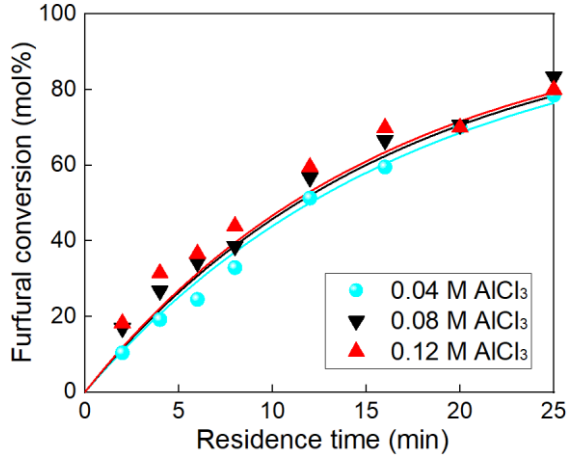

Fig. S13. Effect of acid concentration on the $AlCl_3$-catalyzed furfural conversion. Reaction conditions: *L* = 3.3 m, 160 °C, 0.1 M furfural.

S7.3 Effect of substrate concentration

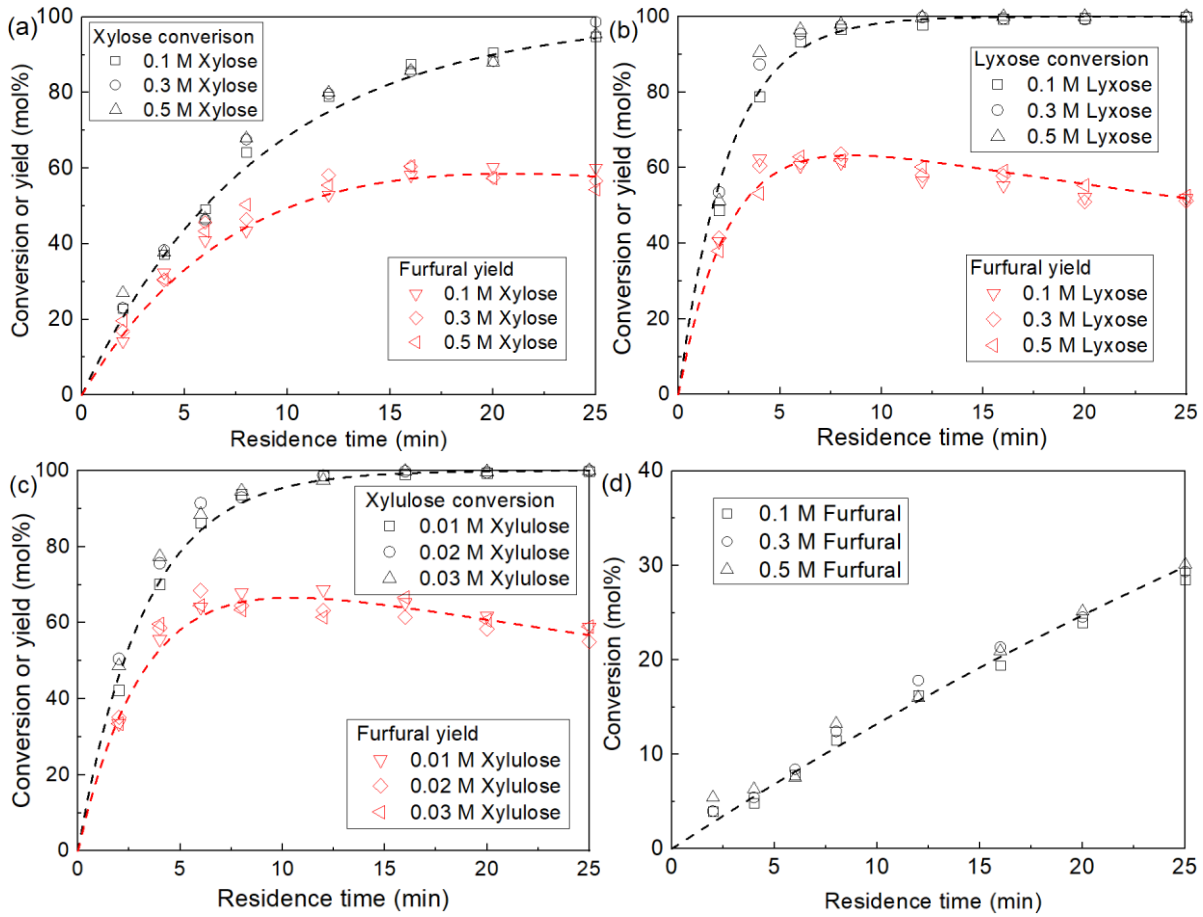

Figure S14. Effect of substrate concentration on the conversion of (a) xylose; (b) lyxose; (c) xylulose; and (d) furfural over HCl with different initial concentrations in monophasic water. Reaction conditions: 200 mM HCl, 160 °C.

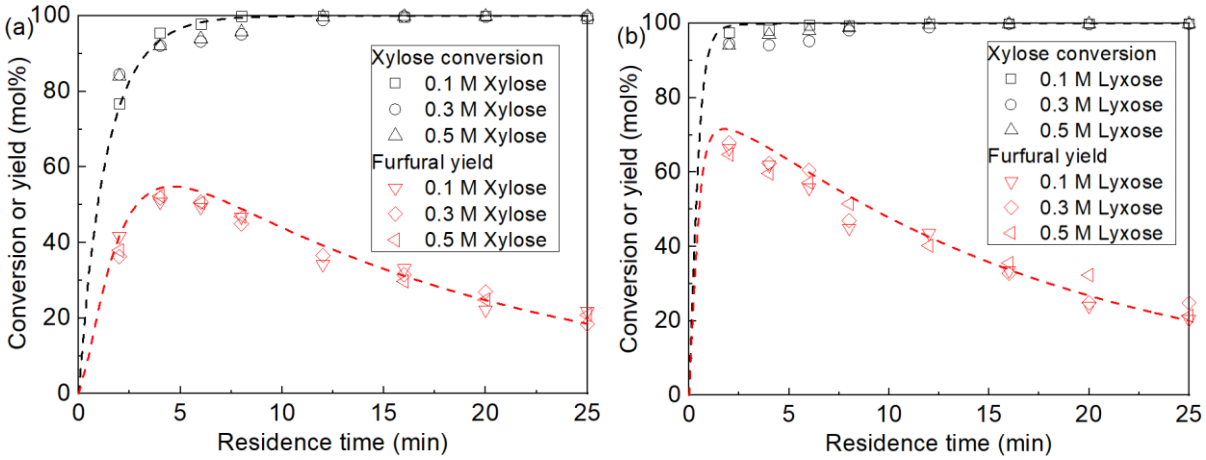

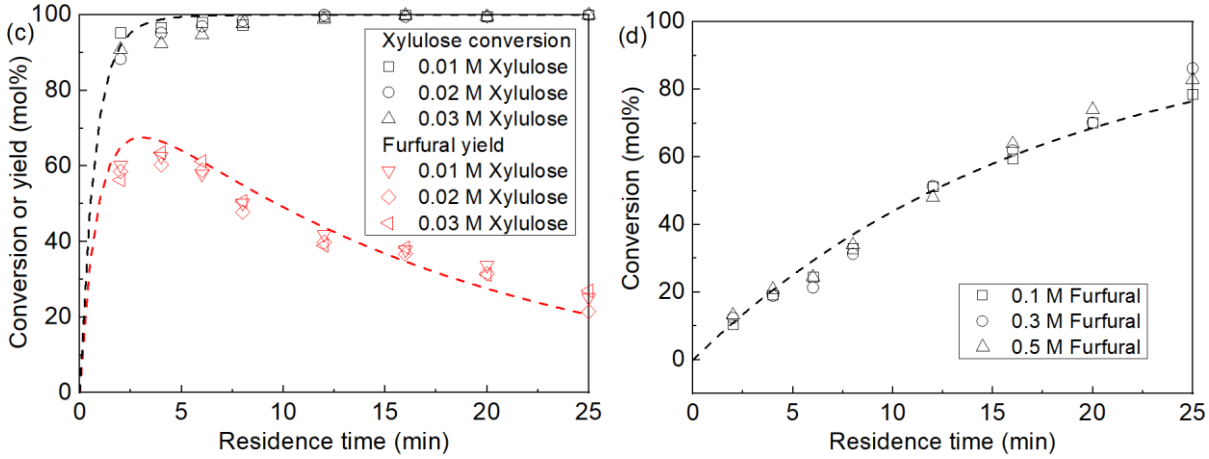

Figure S15. Effect of substrate concentration on the conversion of (a) xylose; (b) lyxose; (c) xylulose; and (d) furfural over $AlCl_3$ with different initial concentrations in monophasic water. Reaction conditions: 40 mM $AlCl_3$, 160 °C.

S7.3 Effect of $AlCl_3$/HCl molar ratio

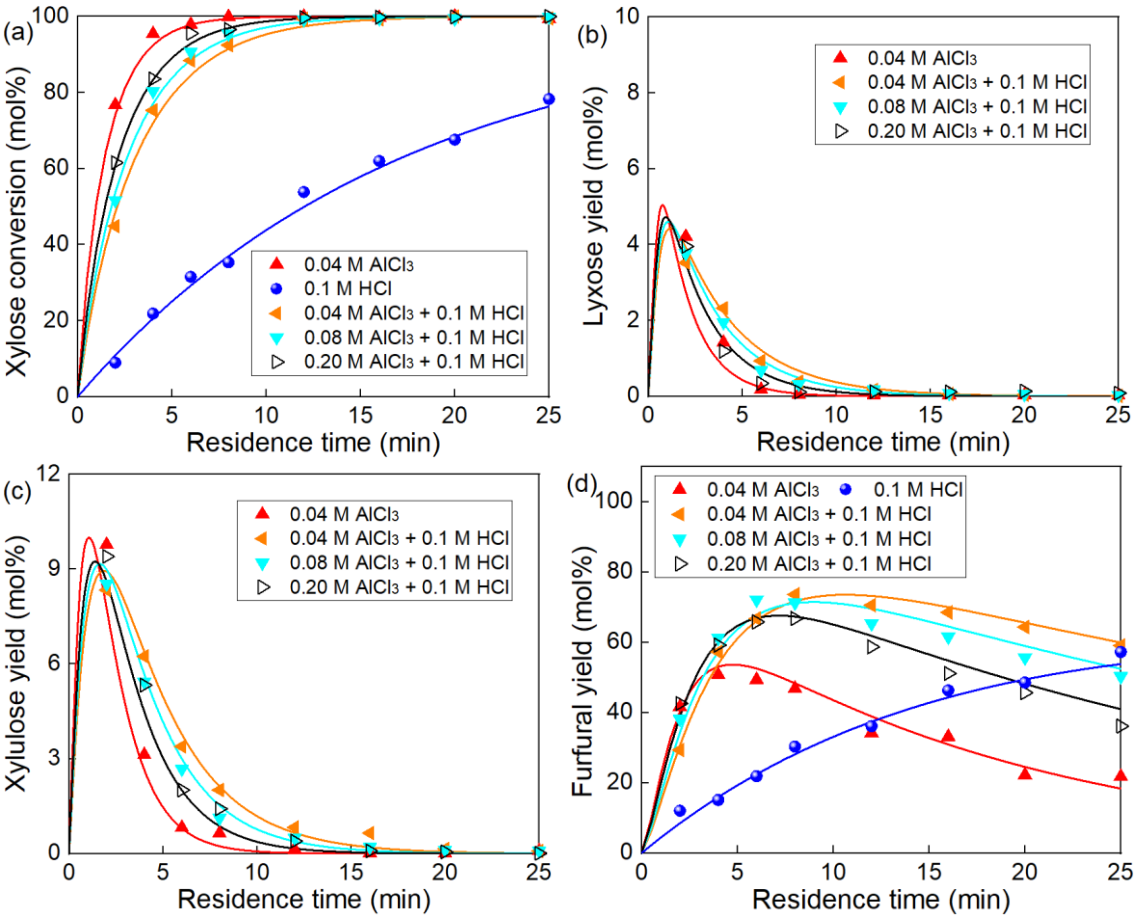

Fig. S16. Effect of $AlCl_3$/HCl molar ratio on (a) xylose conversion and yields of (b) lyxose, (c) xylulose and (d) furfural. Reaction conditions: 160 °C, 0.1 M xylose, monophasic water.

S8. Phase volume change and the concentrations of $Al(OH)_2^+$ and H^+ at reaction temperature

Table S5. Phase volume change and the concentrations of $Al(OH)_2^+$ and H^+ under some representative conditions.

No.	Initial concentration at 20 °C (mM)		T^a (°C)	Volume change ratio		Initial O/A [b]	Actual O/A [c]	Actual concentration at reaction temperature T (mM)			
	$AlCl_3$	HCl		Aq	Org			$AlCl_3$ (mM)	HCl (mM)	$Al(OH)_2^+$ (mM)	H^+ (mM)
1	40	0	120	1.065	-	0	0	37.6	0	0.72	7.1
2	40	0	140	1.086	-	0	0	36.8	0	1.23	11.7
3	40	0	160	1.111	-	0	0	36.0	0	1.93	19.0
4	40	0	180	1.140	-	0	0	35.1	0	2.72	25.6
5	80	0	160	1.111	-	0	0	72.7	0	2.10	26.7
6	120	0	160	1.111	-	0	0	109.1	0	2.18	33.3
7	40	100	120	1.065	-	0	0	37.6	112.7	0.0048	94.4
8	40	100	140	1.086	-	0	0	36.8	110.5	0.0252	93.6
9	40	100	160	1.111	-	0	0	36.0	108.0	0.1102	94.4
10	40	100	180	1.140	-	0	0	35.1	105.3	0.3554	98.3
11	40	100	160	1.115	1.290	1	1.2	35.9	107.7	0.1105	94.1
12	40	100	160	1.047	1.285	2	2.5	38.2	114.6	0.1051	99.9
13	40	100	160	0.974	1.280	3	3.9	41.1	123.3	0.0990	107.1
14	40	100	160	0.909	1.281	4	5.6	44.0	132.1	0.0935	114.5
15	40	100	160	0.488	1.322	8	21.7	82.0	204.9	0.0545	209.6
16	40	100	120	0.931	1.177	4	5.1	43.0	128.9	0.0042	107.9
17	40	100	140	0.920	1.226	4	5.3	43.5	130.4	0.0216	110.2
18	40	100	180	0.895	1.344	4	6.0	44.7	134.0	0.3076	123.0

[a] Reaction temperature; [b] Before mixing and reaction, each phase was fed at 20 °C; [c] After mixing at the reaction temperature and the corresponding saturated vapour pressure.

S9. Additional information regarding the apparent reaction rate constants

Apparent reaction rate constants for the sub-reactions catalyzed by either H^+ ($k_{B,\,ij}^{app}$) or $Al(OH)_2^+$ ($k_{L,\,ij}^{app}$) are defined as the product of intrinsic reaction rate constant ($k_{B,\,ij}$ or $k_{L,\,ij}$) and the corresponding catalyst concentration to a power of reaction order (*n*), and the reaction rates expressions are simplified accordingly, as shown in Table S6.

Table S6. Definition of the apparent reaction rate constants and reaction rates for the sub-reactions within xylose conversion network.

ij	Reaction	Reaction rates	Definition of the apparent rate constants	
			Lewis acid $[Al(OH)_2]^+$	Brønsted acid H^+
1X	Xylose to lyxose[a]	$R_{1X} = k_{L,\,1X}^{app} C_{aq,\,Xylose}$	$k_{L,\,1X}^{app} = k_{L,\,1X} C_{Al(OH)_2^+}^{n_{L,1X}}$	-
2X	Xylose to xylulose[a]	$R_{2X} = k_{L,\,2X}^{app} C_{aq,\,Xylose}$	$k_{L,\,2X}^{app} = k_{L,\,2X} C_{Al(OH)_2^+}^{n_{L,2X}}$	-
3X	Xylose to furfural	$R_{3X} = (k_{L,\,3X}^{app} + k_{B,\,3X}^{app}) C_{aq,\,Xylose}$	$k_{L,\,3X}^{app} = k_{L,\,3X} C_{Al(OH)_2^+}^{n_{L,3X}}$	$k_{B,\,3X}^{app} = k_{B,\,3X} C_{H^+}^{n_{B,3X}}$
4X	Xylose to humins	$R_{4X} = (k_{L,\,4X}^{app} + k_{B,\,4X}^{app}) C_{aq,\,Xylose}$	$k_{L,\,4X}^{app} = k_{L,\,4X} C_{Al(OH)_2^+}^{n_{L,4X}}$	$k_{B,\,4X}^{app} = k_{B,\,4X} C_{H^+}^{n_{B,4X}}$
2L	Lyxose to furfural	$R_{2L} = (k_{L,\,2L}^{app} + k_{B,\,2L}^{app}) C_{aq,\,Lyxose}$	$k_{L,\,2L}^{app} = k_{L,\,2L} C_{Al(OH)_2^+}^{n_{L,2L}}$	$k_{B,\,2L}^{app} = k_{B,\,2L} C_{H^+}^{n_{B,2L}}$
3L	Lyxose to humins	$R_{3L} = (k_{L,\,3L}^{app} + k_{B,\,3L}^{app}) C_{aq,\,Lyxose}$	$k_{L,\,3L}^{app} = k_{L,\,3L} C_{Al(OH)_2^+}^{n_{L,3L}}$	$k_{B,\,3L}^{app} = k_{B,\,3L} C_{H^+}^{n_{B,3L}}$
2Xu	Xylulose to furfural	$R_{2Xu} = (k_{L,\,2Xu}^{app} + k_{B,\,2Xu}^{app}) C_{aq,\,Xylulose}$	$k_{L,\,2Xu}^{app} = k_{L,\,2Xu} C_{Al(OH)_2^+}^{n_{L,2Xu}}$	$k_{B,\,2Xu}^{app} = k_{B,\,2Xu} C_{H^+}^{n_{B,2Xu}}$
3Xu	Xylulose to humins	$R_{3Xu} = (k_{L,\,3Xu}^{app} + k_{B,\,3Xu}^{app}) C_{aq,\,Xylulose}$	$k_{L,\,3Xu}^{app} = k_{L,\,3Xu} C_{Al(OH)_2^+}^{n_{L,3Xu}}$	$k_{B,\,3Xu}^{app} = k_{B,\,3Xu} C_{H^+}^{n_{B,3Xu}}$
1F	Furfural to humins	$R_{1F} = (k_{L,\,1F}^{app} + k_{B,\,1F}^{app}) C_{aq,\,Furfural}$	$k_{L,\,1F}^{app} = k_{L,\,1F} C_{Al(OH)_2^+}^{n_{L,1F}}$	$k_{B,\,1F}^{app} = k_{B,\,1F} C_{H^+}^{n_{B,1F}}$

[a] Corresponding reversible reactions (R_{1L} and R_{1Xu}) were modeled using equilibrium constants calculated from literature[5] (cf. eqn 17, 18 and Table S5).

Table S7. Equilibrium constants for xylose isomerization and epimerization

Reaction	Temperature (°C)	K^a (-)
Xylose ↔ Xylulose	120	0.7448
	140	0.9439
	160	1.1704
	180	1.4239
Xylose ↔ Lyxose	120	0.7278
	140	0.7608
	160	0.7922
	180	0.8218

[a] Equilibrium constants, which are calculated from the kinetic parameters reported in literature[5].

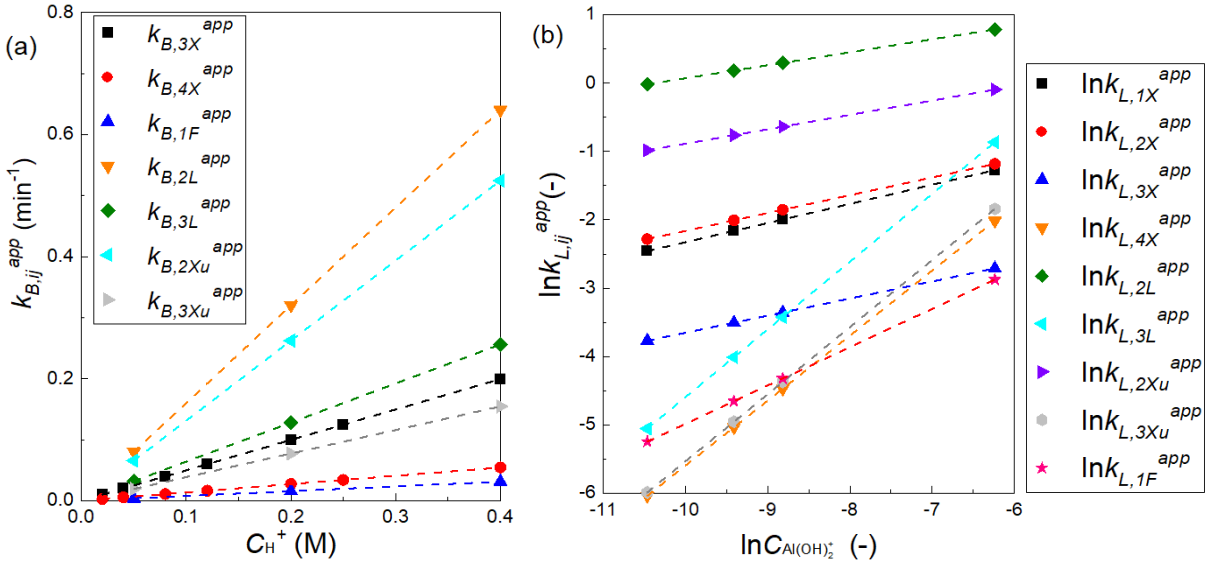

Figure S17. The experimentally determined apparent reaction rate constants for reactions starting from xylose, lyxose, xylulose and furfural versus the concentrations of (a) H^+ and (b) $Al(OH)_2^+$. Reaction conditions: 0.1 M substrate, 160 °C, monophasic water.

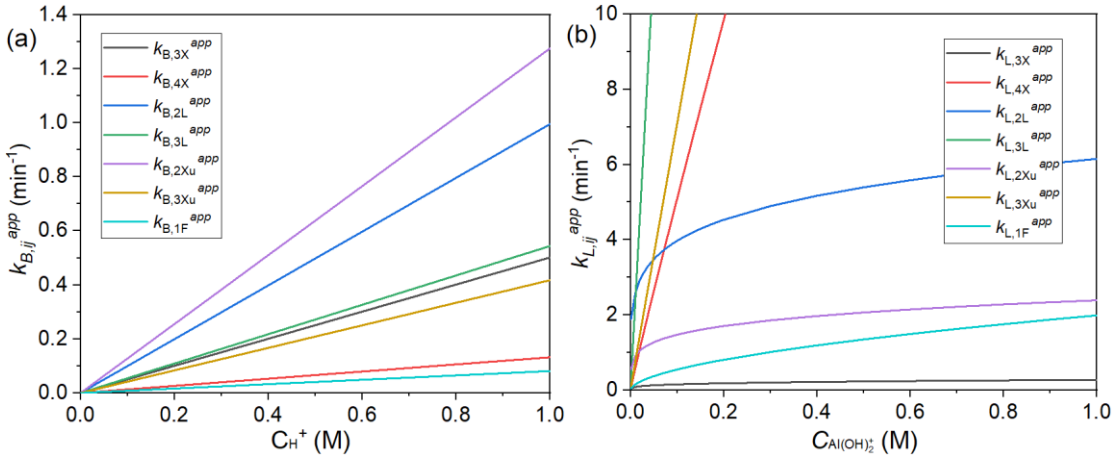

Figure S18. The modeled apparent reaction rate constants (160 °C) for the sub-reactions versus the concentrations of (a) H^+ and (b) $Al(OH)_2^+$.

S10. Partition coefficient of furfural between water and MIBK

Equilibrium furfural concentration was measured in modified pressure tubes (Ace Glass Inc.). Briefly, 1 mL of the aqueous phase containing 0.1 M furfural and 1 mL of MIBK were added into the tube, followed by sealing and heating in an oil bath at a set temperature under stirring at 800 rpm for 2 h to reach equilibrium. The actual reaction temperature was monitored by a calibrated thermocouple inserted into the sealed tube. Afterwards, ca. 0.5 mL of the aqueous or organic phase was sampled from the tube at the reaction temperature. The collected sample was cooled (to 20 °C) and analyzed with HPLC for the aqueous phase or GC for the organic phase (cf. Section 2.3).

The partition coefficient of furfural at the reaction temperature was defined as

$$m = \frac{C_{\text{org, furfural, eq}}}{C_{\text{aq, furfural, eq}}} \quad \text{(S9)}$$

where $C_{\text{org, furfural, eq}}$ and $C_{\text{aq, furfural, eq}}$ are the respective equilibrium furfural concentrations in organic and aqueous phase at the reaction temperature. It should be noted that due to the volume change after cooling of the samples before analysis, the actual furfural concentration at the reaction temperature differs from the measured concentrations at 20 °C, which should be corrected by taking this volume change into account for the calculation of the partition coefficient (cf. details in our previous work[2, 3]).

Fig. S18 shows the measured *m* values at different reaction temperatures, which can be well fitted using the following linear regression equation

$$m = a - bT \quad \text{(S10)}$$

where a = 10.137, b = 0.0154, and T is in °C.

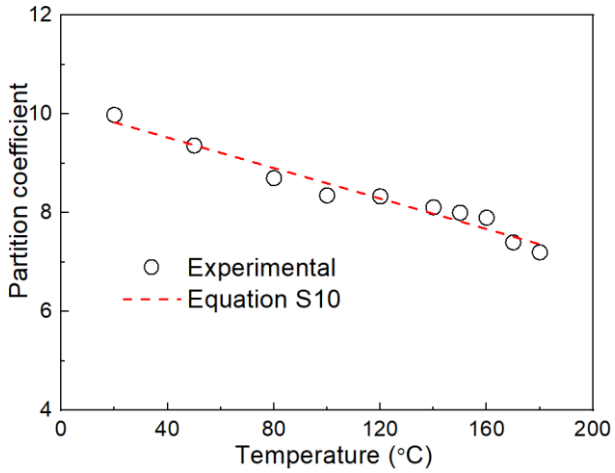

Fig. S19. Partition coefficient of furfural between water and MIBK as a function of the reaction temperature.

S11. Mass transfer efficiency in the slug flow microreactor

For a given extraction O/A and *m* in the biphasic system, the mass transfer efficiency is dependent on the mass transfer coefficient (K_La). Under the slug flow operation in microreactors, furfural is transferred from aqueous droplets to organic slugs through (i) the caps of the droplets and (ii) the MIBK film between the droplet and reactor wall. To estimate the mass transfer coefficient, it is crucial to understand the extraction pathways and their significance. The contribution of each pathway is reflected on the Fourier number (Fo), which is defined as the ratio of the contact time of the aqueous droplet with the surrounding organic film, to the time for film saturation.

$$Fo = \frac{L_{film} D_{org}}{U_{slug} \delta_{film}^2} \quad \text{(S11)}$$

where L_{film} is the film length (measured in Fig. S19a). D_{org} is the diffusivity of furfural in MIBK phase. U_{slug} is the superficial velocity of the slugs. δ_{film} is the film thickness, which can be estimated from the following semi-empirical relation[6]

$$\frac{\delta_{film}}{d_C} = \frac{0.66Ca^{2/3}}{1+0.33Ca^{2/3}} \tag{S12}$$

where d_C is the inner diameter of microreactor tube. *Ca* is the capillary number defined by

$$Ca = \frac{\mu_{MIBK} U_{slug}}{\sigma_{water\text{-}MIBK}} \tag{S13}$$

where μ_{MIBK} is the dynamic viscosity of the continuous phase MIBK, and $\sigma_{water\text{-}MIBK}$ is the interfacial tension between water and MIBK.

For all experiments, the calculated film thickness δ_{film} ranges from 0.98 to 11.8 μm, and *Fo* ranges from 1.16 to 7.4 × 10^3. Such large *Fo* number indicates a fast saturation of the thin film due to the long contact time. Therefore, the dominant pathway for furfural mass transfer is through the caps of the droplets, and the mass transfer coefficient K_L can be estimated from[7]

$$K_L = \frac{1}{\frac{1}{\frac{2\sqrt{2}}{\pi}\sqrt{\frac{D_{aq}U_{slug}}{d_c}}} + \frac{1}{m\frac{2\sqrt{2}}{\pi}\sqrt{\frac{D_{org}U_{slug}}{d_c}}}} \tag{S14}$$

where D_{aq} is the diffusion coefficients of furfural in aqueous phase.

The values of all the physical properties mentioned in the above equations can be found in our previous work.[3]

The specific interfacial area of the cap region was calculated according to the slug flow image in Fig. S19a. The lengths of droplet, slug and cap (denoted as L_{D}, L_{S} and L_{cap},

respectively) were measured. The cap is assumed to be of the oblate spheriod shape with three elliptic radii being approximated as $d_C/2$, $d_C/2$, and L_{cap} (Fig. S19a). Thus, there is

$$a_{cap} = \frac{\frac{\pi}{2} d_C^{\,2} + \pi \frac{L_{cap}^{\,2}}{e} ln(\frac{1+e}{1-e})}{\frac{\pi}{4} d_C^{\,2} (L_D + L_S)} \tag{S15}$$

where, *e* is the ellipticity of the oblate spheriod and defined as

$$e = \sqrt{\left(\frac{d_C^{\,2}}{4}\right) - L_{cap}^{\,2}} \Big/ \frac{d_C}{2} \tag{S16}$$

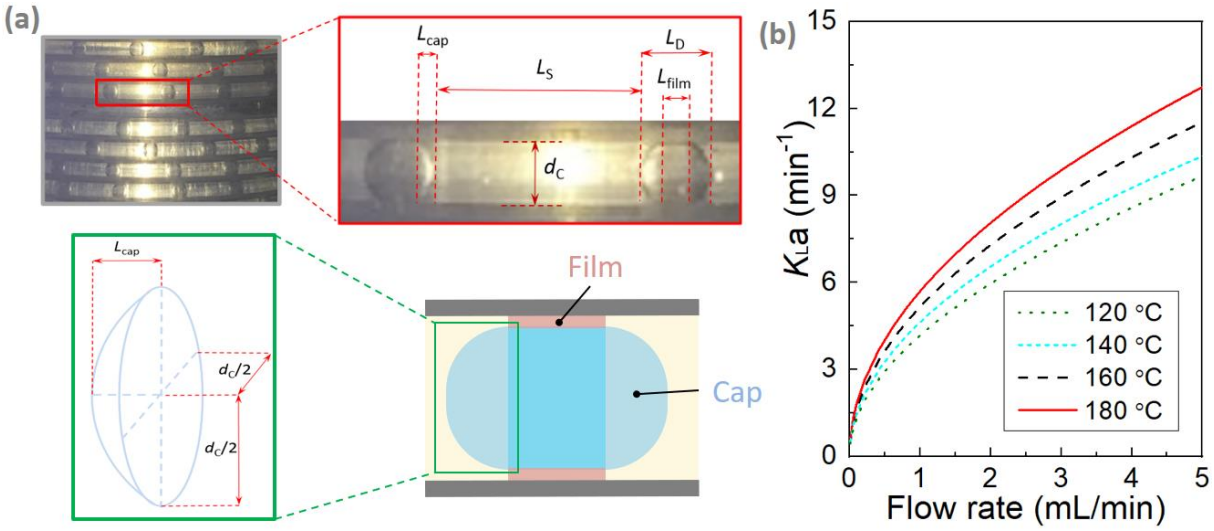

Fig. S20. (a) Imagine of the slug flow in the present PFA microreactor (O/A = 4); (b) Estimated mass transfer coefficients as a function of the flow rate at the microreactor inlet (water-MIBK biphasic system, O/A = 4).

The calculated mass transfer coefficient $K_L a$ is presented in Fig. S19b. Apparently, $K_L a$ is a strong function of the flow rate, as higher superficial velocity enhances the inner circulation in the droplets and slugs, and thus largely promotes the furfural extraction rates. Increase of temperature leads to higher $K_L a$, due to the higher diffusivity of furfural in water and MIBK at higher temperature.

The calculation results (Fig. S20b) and literature suggest that higher flow rates (or equivalently, higher droplet/slug velocity) lead to higher mass transfer coefficients, as a result of the enhanced inner circulation in the droplets and slugs.[8-10] As such, a higher furfural yield is expected in longer microreactors if the mass transfer limitation is present. Here, the xylose reactions were performed in microreactors of different lengths (1.2, 3.3 and 16.9 m) to investigate the mass transfer efficiency under slug flow. Different flow rates were applied to maintain the same residence time for the different microreactor lengths, and the corresponding k_La were calculated as displayed in Fig. S21a. Generally, longer microreactors give higher k_La, and all the calculated k_La values are two order of magnitude greater than the apparent rate constant of furfural degradation ($k_{L,\,1F}^{app} = 0.0092\,\mathrm{min}^{-1}$ and $k_{L,\,1B}^{app} = 0.011\,\mathrm{min}^{-1}$ at 160 °C with 40 mM $AlCl_3$ and 200 mM HCl). Furthermore, the reaction results in Figs. S21 b and c show minor differences in xylose conversion and furfural yield among different reactor lengths. Consequently, both the calculation and experimental results indicate that the interfacial mass transfer resistance was largely eliminated and the reaction was performed predominantly in the kinetic regime.

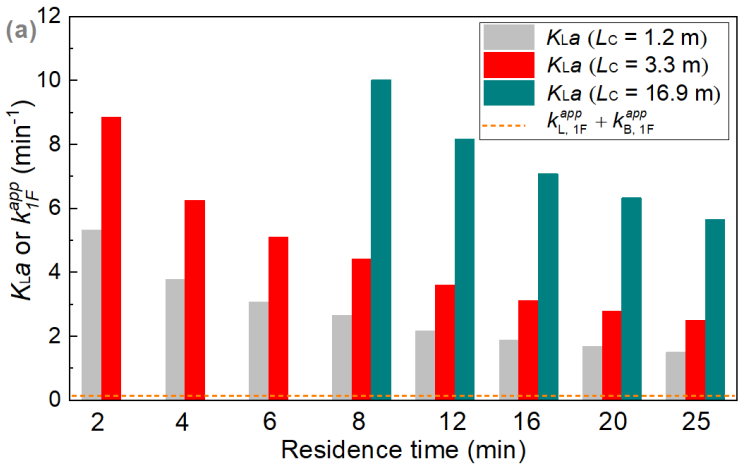

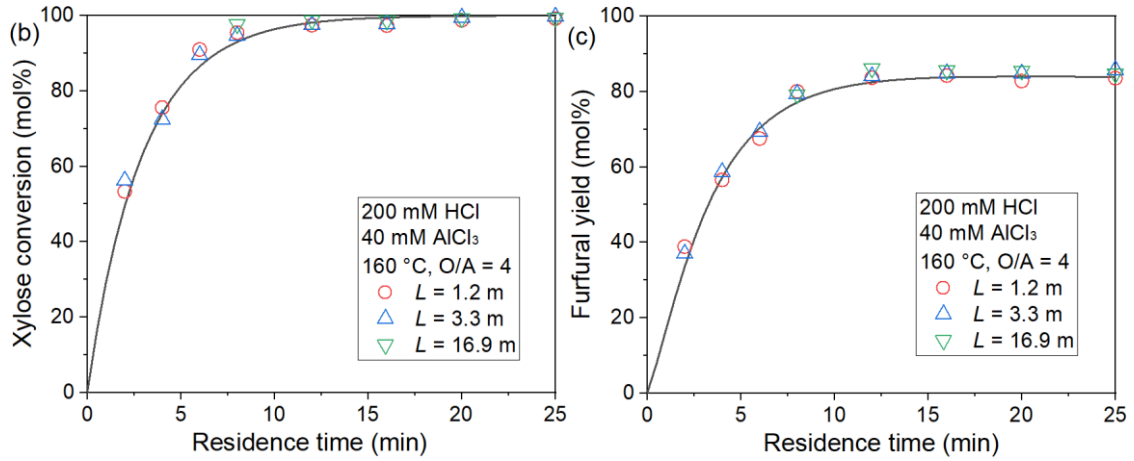

Fig. S21. (a) the estimated mass transfer coefficient; (b) xylose conversion and (c) furfural yield as a function of residence time in the slug flow microreactor with different lengths. Conditions: 160 °C, 40 mM $AlCl_3$, 200 mM HCl, O/A = 4.

S12. Parity plot for model predictions and experiment results

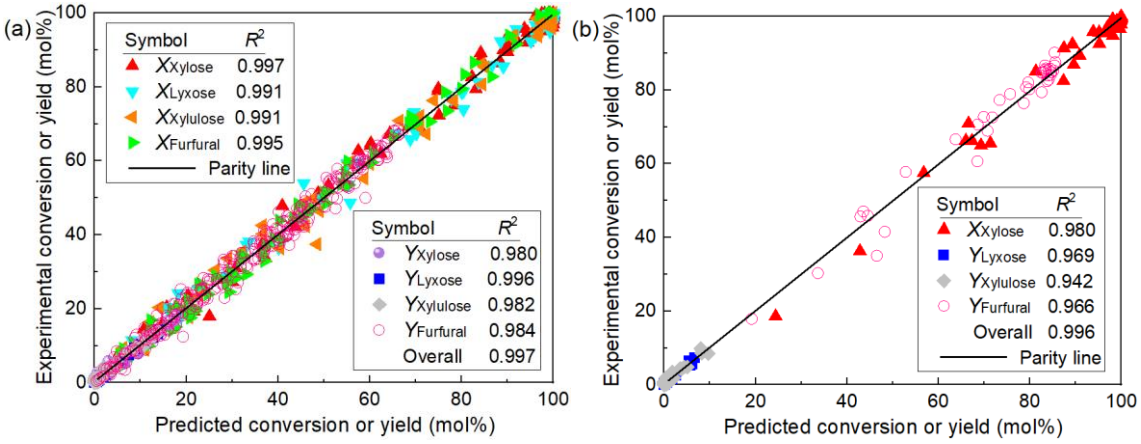

Fig. S22. Parity plots for the model predications and experimental results for the conversion and yield of all components in (a) monophasic water and (b) biphasic water-MIBK solvent system in the microreactor.

S13. Effect of temperature on the sugar conversion over sole $Al(OH)_2^+$ or H^+ in water

To study the effect of temperature on the individual H^+-catalyzed and $[Al(OH)_2]^+$-catalyzed reactions, the conversion of xylose and the corresponding product yields as function of residence time at varying temperatures were modelled based on the developed kinetic model.

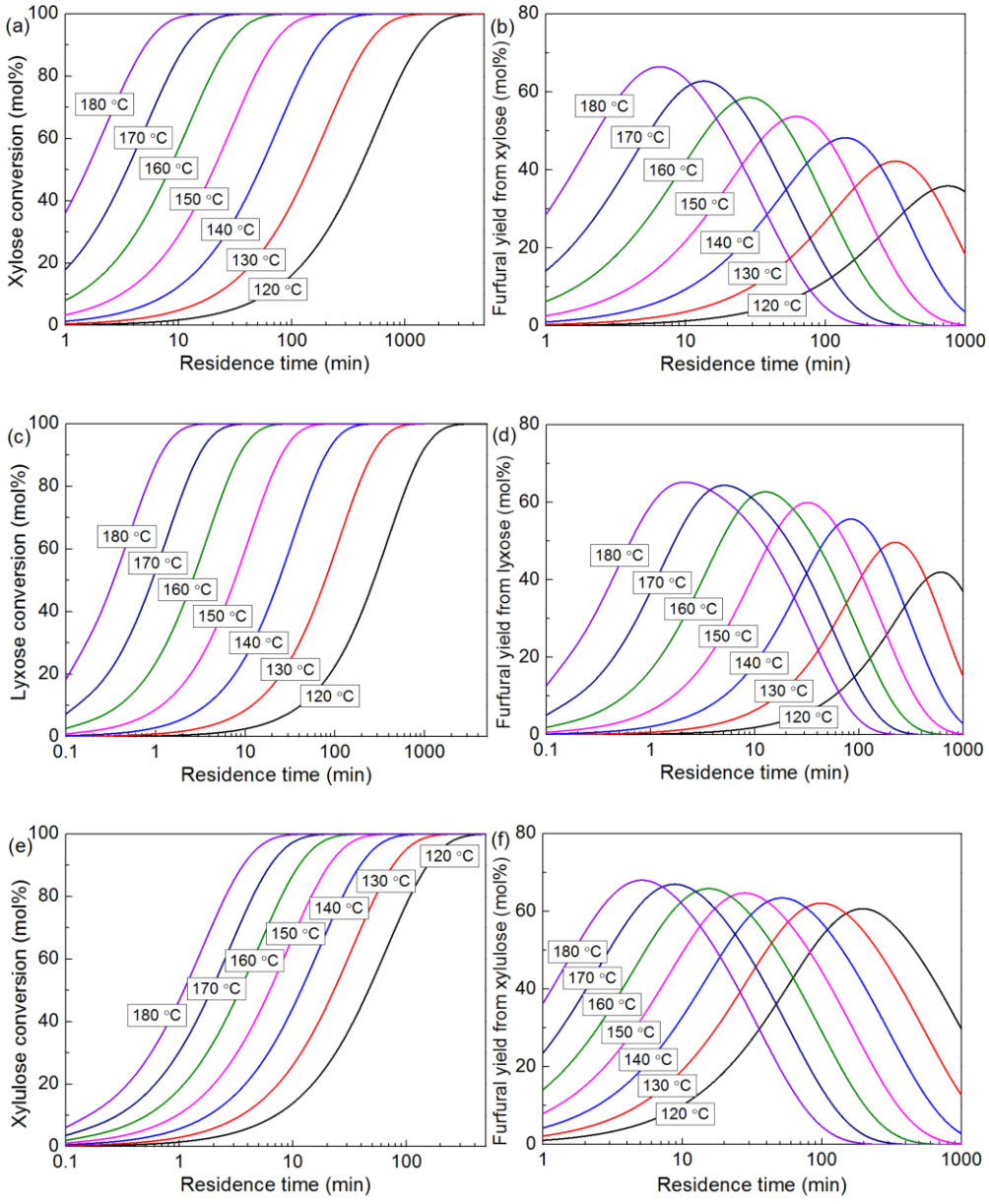

Figure S23. Effect of temperature on the H^+-catalyzed (a) xylose conversion and (b) furfural yield from xylose; (c) lyxose conversion and (d) furfural yield from lyxose; and (e) xylulose conversion and (f) furfural yield from xylulose. Reaction conditions: 0.12 M H^+, 0.5 M substrate, monophasic water.

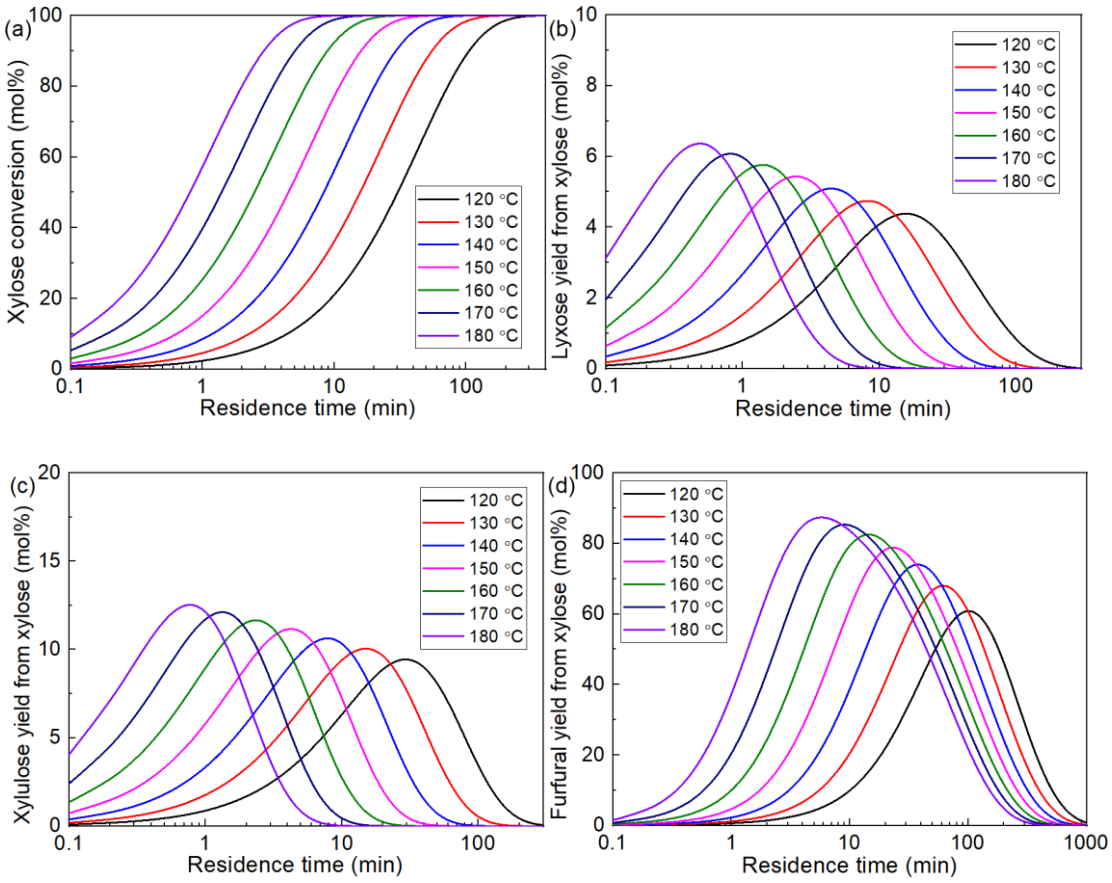

Figure S24. Effect of temperature on the $[Al(OH)_2]^+$-catalyzed (a) xylose conversion; (b) lyxose yield; (c) xylulose yield and (d) furfural yield at varying reaction temperatures. Reaction conditions: 0.1 mM $[Al(OH)_2]^+$, 0.5 M xylose, monophasic water.

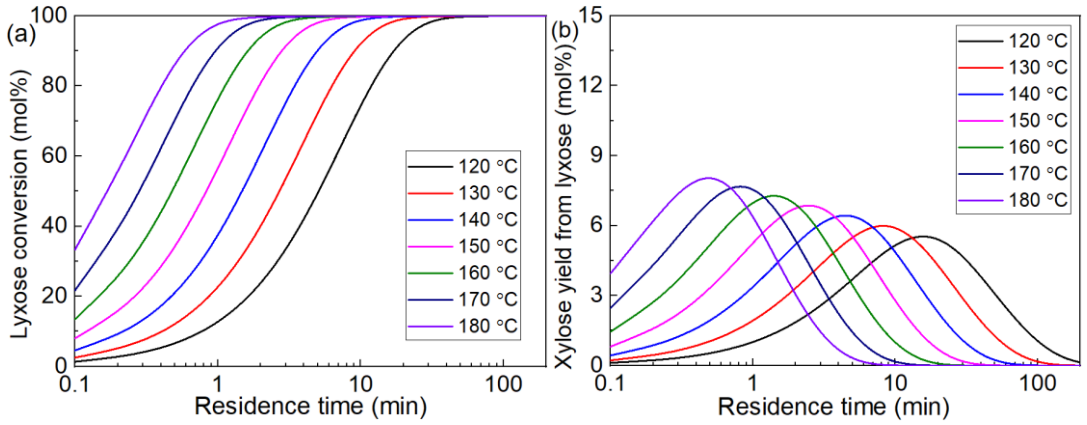

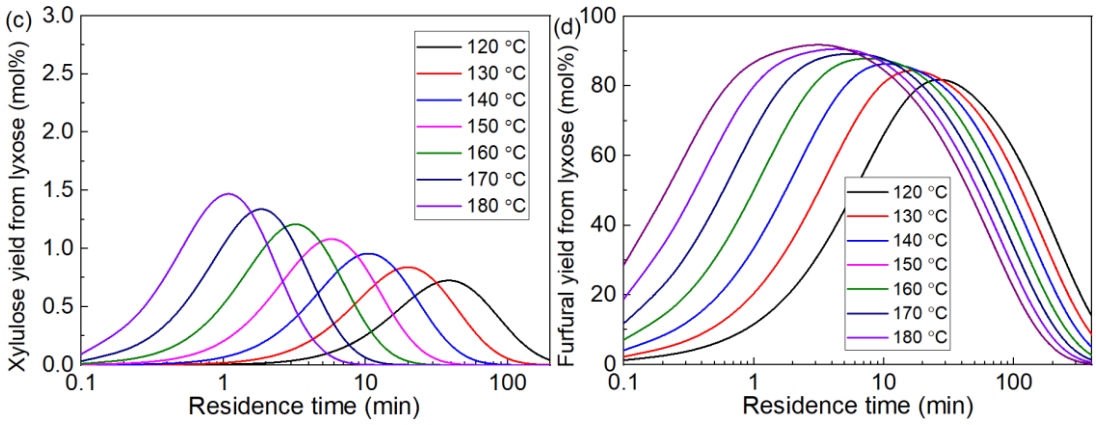

Figure S25. Effect of temperature on the $[Al(OH)_2]^+$-catalyzed (a) lyxose conversion; (b) xylose yield; (c) xylulose yield and (d) furfural yield at varying reaction temperatures. Reaction conditions: 0.1 mM $[Al(OH)_2]^+$, 0.5 M lyxose, monophasic water.

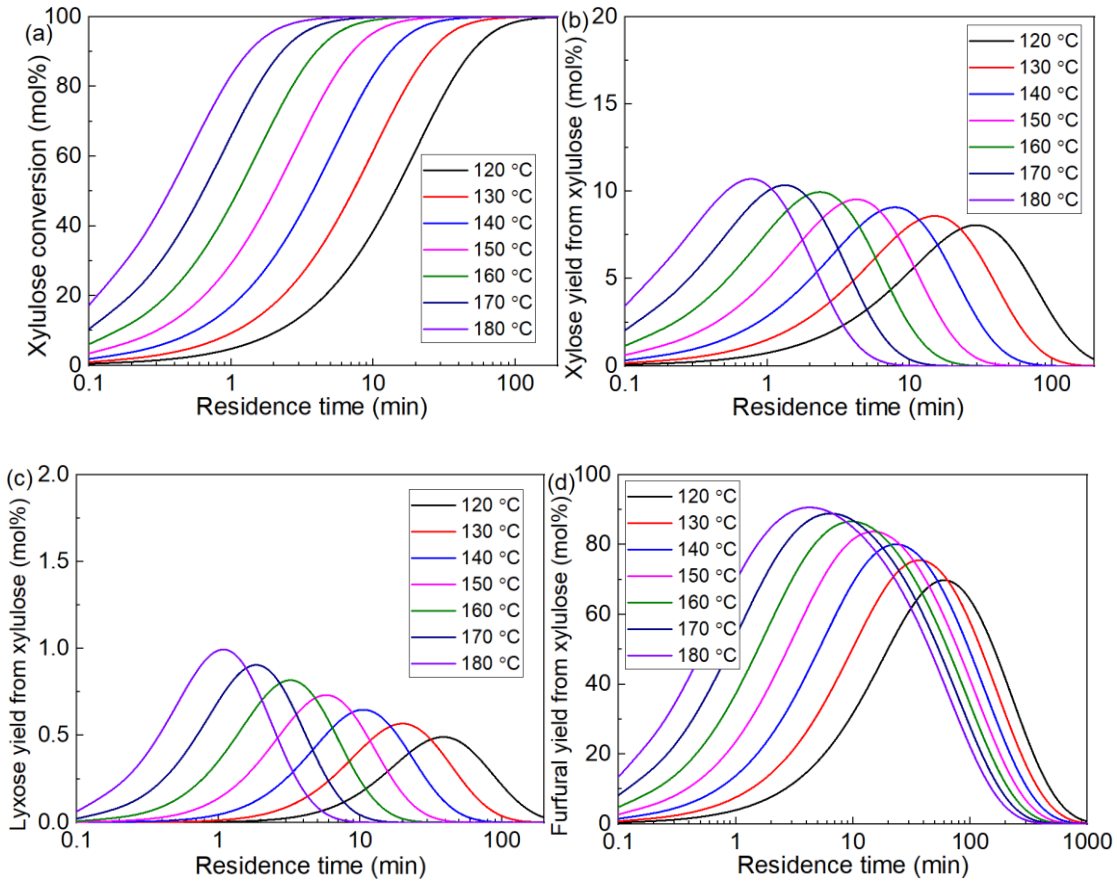

Figure S26. Effect of temperature on the $[Al(OH)_2]^+$-catalyzed (a) xylulose conversion; (b) xylose yield; (c) lyxose yield and (d) furfural yield at varying reaction temperatures. Reaction conditions: 0.1 mM $[Al(OH)_2]^+$, 0.5 M xylulose, monophasic water.

S14. Analysis of humin sources and furfural yields

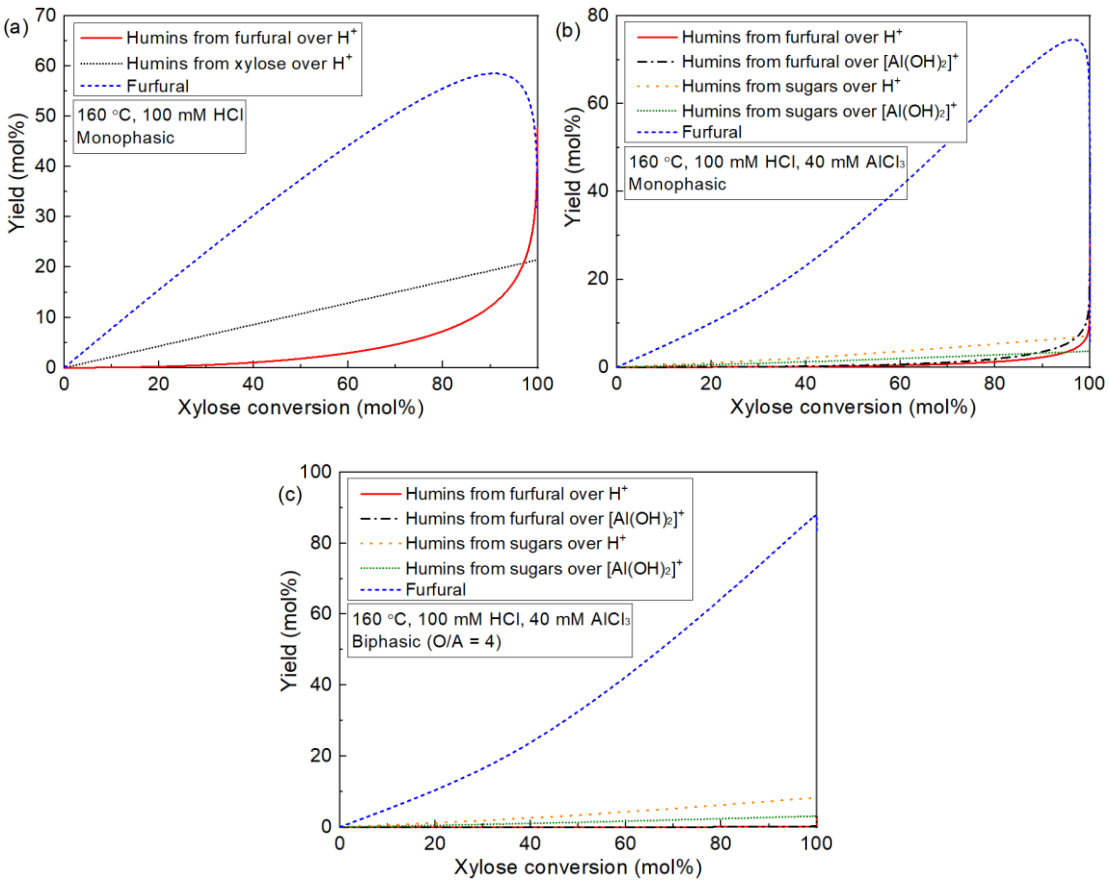

Figure S27. Analysis of humin sources and furfural yields under different conditions. (a) 100 mM HCl in monophasic water; (b) 100 mM HCl and 40 mM $AlCl_3$ in monophasic water; and (c) 100 mM HCl and 30 mM $AlCl_3$ in biphasic water-MIBK system. Other conditions: L = 3.3 m, 160 °C, 0.1 M xylose.

S15. Performance of literature work on furfural synthesis from xylose and their comparison with this work

Table S8. Performance on furfural synthesis from xylose in water in the literature and this work.

No	Catalyst	Solvent system	Reactor	$C_{Xyl,0}$ [a] (wt%)	T [b] (°C)	Time [c] (min)	$Y_{Furfural}$ [d] (mol%)	$STY_{Furfural}$ [e] (mol min^{-1} m^{-3})	Work
1	CO_2	Water/THF-MIBK	Batch reactor	1.25	180	60	56.6	0.037	Morais et al.[11,12]
2	Nb_2O_5/SBA-15	Water/toluene	Batch reactor	2	160	1440	78	0.036	García-Sancho et al.[13]
3	Arenesulfonic SBA-15	Water/toluene	Batch reactor	2	160	1200	80	0.044	Agirrezabal-Telleria et al.[14]
4	Amberlyst-70	Water/toluene	Batch reactor	1	175	240	54	0.084	Arias et al.[15]
5	H-ZSM-5	Water/toluene	Batch reactor	3	140	240	42.8	0.107	Kim et al.[16]
6	SO_4^{2-}/ZrO_2/MCM-41	Water/toluene	Batch reactor	10	160	240	43	0.358	Dias et al.[17]
7	MCM-41-Nb	NaCl-water/toluene	Batch reactor	10	170	180	59.9	0.666	García-Sancho et al.[18]
8	NbP	Water/toluene	Batch reactor	10	210	60	70	3.241	Pholjaroen et al.[19]
9	$AlCl_3$	NaCl-water/THF	Batch reactor	3.75	140	45	75	1.042	Yang et al.[20]
10	HCl	Water/MIBK	Batch reactor	10	170	30	75	7.408	Weingarten et al.[21]
11	H_2SO_4	Water/toluene	Slug flow millireactor	4	190	2.5	56	19.89	Papaioannou et al.[22]
12	HCl [f,g]	NaCl-water/MIBK	Slug flow microreactor	15	160	12	91.8	11.87	Guo et al.[3]
13	HCl [f,g]	NaCl-water/MIBK	Slug flow microreactor	15	180	4	92.7	35.96	Guo et al.[3]
14	$AlCl_3$+HCl [g]	Water/MIBK	Slug flow microreactor	15	160	12	90	11.64	This work

[a] Initial concentration of xylose. [b] Reaction temperature. [c] Reaction time in the batch reactor or residence time in the microreactor. [d] Furfural yield. [e] The space time yield of furfural ($STY_{Furfural}$) in the batch reactor is determined by $STY_{Furfural} = N_{Xylose,0} Y_{Furfural} / (V_L t)$, where $N_{Xylose,0}$ is the initial mole amount of xylose, V_L is the total liquid volume in the reactor and t is the reaction time. The $STY_{Furfural}$ of furfural in the continuous flow millreactor or microreactor is calculated by $STY_{Furfural} = \frac{Q_{aq,1} C_{aq,Furfural,1} + Q_{org,1} C_{org,Furfural,1}}{\pi (d_C / 2)^2 L_C} \times 100\%$, where $C_{aq,Furfural,1}$ and $C_{org,furfural,1}$ are the concentrations of furfural in the aqueous and organic phase, respectively, at the reactor outlet (at ca. 20 °C), d_C and L_C are the inner diameter and length of the reactor, respectively. [f] With the addition of 10 wt% NaCl in the aqueous phase. [g] With 1 M xylose feedstock solution.

Reference

1. W. Guo, H. J. Heeres and J. Yue, *Chemical Engineering Journal*, 2020, **381**, 122754.
2. W. Guo, Z. Zhang, J. Hacking, H. J. Heeres and J. Yue, *Chemical Engineering Journal*, 2021, **409**, 128182.
3. W. Guo, Doctoral dissertation, University of Groningen, 2021.
4. W. L. Bourcier, K. G. Knauss and K. J. Jackson, *Geochimica et cosmochimica acta*, 1993, **57**, 747-762.
5. I. Delidovich, M. S. Gyngazova, N. Sánchez-Bastardo, J. P. Wohland, C. Hoppe and P. Drabo, *Green Chemistry*, 2018, **20**, 724-734.
6. P. Aussillous and D. J. P. o. f. Quéré, *Physics of Fluids*, 2000, **12**, 2367-2371.
7. J. M. van Baten and R. Krishna, *Chemical Engineering Science*, 2004, **59**, 2535-2545.
8. D. Tsaoulidis and P. Angeli, *Chemical Engineering Journal*, 2015, **262**, 785-793.
9. M. N. Kashid, I. Gerlach, S. Goetz, J. Franzke, J. F. Acker, F. Platte, D. W. Agar and S. Turek, *Industrial & Engineering Chemistry Research*, 2005, **44**, 5003-5010.
10. T. Shimanouchi, Y. Kataoka, T. Tanifuji, Y. Kimura, S. Fujioka and K. Terasaka, *AIChE Journal*, 2016, **62**, 2135-2143.
11. A. R. C. Morais, M. D. D. J. Matuchaki, J. Andreaus and R. Bogel-Lukasik, *Green Chemistry*, 2016, **18**, 2985-2994.
12. A. R. C. Morais and R. Bogel-Lukasik, *Green Chemistry*, 2016, **18**, 2331-2334.
13. C. García-Sancho, I. Agirrezabal-Telleria, M. B. Güemez and P. Maireles-Torres, *Applied Catalysis B: Environmental*, 2014, **152-153**, 1-10.
14. I. Agirrezabal-Telleria, J. Requies, M. B. Güemez and P. L. Arias, *Applied Catalysis B: Environmental*, 2014, **145**, 34-42.
15. I. Agirrezabal-Telleria, A. Larreategui, J. Requies, M. B. Güemez and P. L. Arias, *Bioresource Technology*, 2011, **102**, 7478-7485.
16. S. B. Kim, S. J. You, Y. T. Kim, S. Lee, H. Lee, K. Park and E. D. Park, *Korean Journal of Chemical Engineering*, 2011, **28**, 710-716.
17. A. S. Dias, S. Lima, M. Pillinger and A. A. Valente, *Catalysis Letters*, 2007, **114**, 151-160.

18. C. García-Sancho, I. Sádaba, R. Moreno-Tost, J. Mérida-Robles, J. Santamaría-González, M. López-Granados and P. Maireles-Torres, *ChemSusChem*, 2013, **6**, 635-642.

19. B. Pholjaroen, N. Li, Z. Wang, A. Wang and T. Zhang, *Journal of Energy Chemistry*, 2013, **22**, 826-832.

20. Y. Yang, C.-W. Hu and M. M. Abu-Omar, *ChemSusChem*, 2012, **5**, 405-410.

21. R. Weingarten, J. Cho, J. W. C. Conner and G. W. Huber, *Green Chemistry*, 2010, **12**, 1423-1429.

22. M. Papaioannou, R. J. T. Kleijwegt, J. van der Schaaf and M. F. Neira d'Angelo, *Industrial & Engineering Chemistry Research*, 2019, **58**, 16106-16115.